XJ97A0064

ISSN 0234-5366

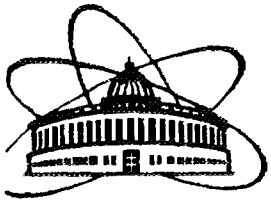

КРАТКИЕ СООБЩЕНИЯ ОИЯИ

JINR RAPID COMMUNICATIONS

6[80]-96

Издательский отдел ОИЯИ ДУБНА

JINR Publishing Department DUBNA

РЕДАКЦИОННЫЙ СОВЕТ

А.М.Балдин — председатель
А.Н.Сисакян — зам.председателя
Д.В.Ширков — зам.председателя
С.Г.Стеценко — ученый секретарь

В.А.Бедняков
А.А.Бельков
В.А.Бирюков
С.Дубничка
В.И.Журавлев
И.Звара
П.И.Зарубин
П.С.Исаев
И.Натканец
Б.И.Пустыльник
В.В.Сиколенко
Т.А.Стриж
— члены совета

EDITORIAL BOARD

A.M.Baldin — Chairman
A.N.Sissakian — Vice-Chairman
D.V.Shirkov — Vice-Chairman
S.G.Stetsenko — Scientific Secretary

V.A.Bednyakov
A.A.Belkov
V.A.Biryukov
S.Dubnicka
V.I.Zhuravlev
I.Zvara
P.I.Zarubin
P.S.Isaev
I.Natkaniec
B.I.Pustylnik
V.V.Sikolenko
T.A.Strizh
— Members of the Board

© Объединенный институт ядерных исследований. Дубна, 1996

Объединенный институт ядерных исследований
Joint Institute for Nuclear Research

6[80]-96

КРАТКИЕ СООБЩЕНИЯ ОИЯИ

JINR RAPID COMMUNICATIONS

Дубна 1996

В журнале *«Краткие сообщения ОИЯИ»* публикуются статьи, содержащие оригинальные результаты теоретических, экспериментальных, научно-технических, методических и прикладных исследований. Содержание публикуемых статей определяется тематикой научных исследований в ОИЯИ: теоретическая физика, физика элементарных частиц, релятивистская ядерная физика, физика тяжелых ионов, ядерная физика низких и промежуточных энергий, нейтронная ядерная физика, физика конденсированных сред, радиационная биология и медицина, экспериментальные методы и установки, а также прикладные исследования.

Журнал зарегистрирован в Комитете Российской Федерации по печати, издателем журнала является Объединенный институт ядерных исследований.

Журнал выходит шесть раз в год.

The journal *JINR Rapid Communications* publishes the articles providing information on original results of theoretical, experimental, scientific-technical, methodical and applied investigations. Subject-matter of articles covers the principal fields of research at JINR: theoretical physics, elementary particle physics, relativistic nuclear physics, heavy ion physics, low- and intermediate-energy physics, neutron nuclear physics, condensed matter physics, radiation biology and medicine, experimental instruments and methods and applied research.

The journal is registered in the Committee of the Russian Federation for Press and is published bimonthly by the Joint Institute for Nuclear Research.

References to the articles of the *JINR Rapid Communications* should contain:

— names and initials of authors,
— title of journal, introduced by word "In:",
— year of publication,
— publication index,
— page number.

For example:
Batyunya B.V., Zinchenko A.I. — JINR Rapid Communications, 1995, No.3[71]-95, p.5.

ОГЛАВЛЕНИЕ
CONTENTS

XJ9700064

УДК 539.12.01

THE CHARACTER OF METASTABLE STATES OF THE ANTIPROTONIC HELIUM

A.V.Matveenko, H.Fukuda*

A simple semianalytic wave function for «the Atomcule» — metastable state of the antiprotonic helium — is derived using body-fixed hyperspherical coordinates:

$$\Psi^J(R, \xi, \eta, \tilde{\alpha}, \beta, \gamma) = R^J[c_1(R) \sin^J\alpha_a \, e^{-\sqrt{-\epsilon_n}x_a} P_J(\omega_a) +$$

$$+ c_2(R) \cos^J \alpha_b \, e^{-\sqrt{-\epsilon_1}x_b} P_J(\omega_b - \theta_b)] B_0^J(\gamma, \beta, \tilde{\alpha}),$$

where $B_0^j(\gamma, \beta, \tilde{\alpha})$ is σ-projection of the rotational motion, α_i and θ_i are the usual two-body-channel hyperspherical angles, $\cos\omega_a = \hat{\omega} \cdot \hat{x}_a$ defines the angle fixing the position of the inertia tensor principal axis $\hat{\omega}$ in the particle triangle plane with respect to one of its sides x_a (same for ω_b). Formally this expression is the well-known linear combination of two approximately resonant hydrogenic orbitals: the novel position is their angular part that exhibits the common pure rotational (dynamic) component $B_0^j(\gamma, \beta, \tilde{\alpha})$ and the kinematic part coupling together collective (ω_i) and channel (θ_i) angles in a general case. Hyperradius R and ξ, η are internal dynamic variables.

As lower lying states of $\bar{p}He^+$ have the configuration of the ground one, i.e., the product of two hydrogenic orbitals, all they have a rather different character. This determines the longevity of high angular momentum molecular states.

The investigation has been performed at the Bogoliubov Laboratory of Theoretical Physics, JINR.

Характер метастабильных состояний антипротонного гелия

А.В.Матвеенко, Х.Фукуда

Получена простая полуаналитическая волновая функция для метастабильных состояний антипротонного гелия. Используются гиперсферические координаты с осью квантования, направленной вдоль одной из главных осей тензора инерции системы трех частиц. Выбор оси квантования позволяет факторизовать вращательную составляющую волновой функции. Ее оставшаяся часть имеет вид обычной молекулярной орбитали; новым моментом является характерная зависимость атомных орбиталей от так называемых «внутренних углов», которыми в данном случае являются: угол между парой якобиевских векторов, а также угол, задающий положение главной оси тензора инерции.

*School of Administration and Informatics, University of Shizuoka, Yada 52-1, Shizuoka-shi, Shizuoka 422, Japan

Поскольку состояния, лежащие ниже, имеют главным образом конфигурацию основного состояния (произведение атомных орбиталей), автоматически решается вопрос о метастабильности данных состояний (линейной комбинации атомных орбиталей).

Работа выполнена в Лаборатории теоретической физики им. Н.Н.Боголюбова ОИЯИ.

Recently observed laser-induced transitions in antiprotonic helium atoms [1] unambiguously demonstrated that the anomalous longevity of antiprotons results from the formation of high angular momentum states of $\bar{p}He^+$ [2,3]. The full variational calculation [4] of the corresponding Coulombic three-body problem has practically reproduced the observed transitions. On the other hand, there are many experimental findings that have not been explained theoretically. Among them are phase and density effects, isotopic effect and quenching by foreign gases [1]. Though it is widely believed that the formation of the exotic system is due to an atomic electron replacement by the incoming antiproton, there is neither direct experimental information nor reliable theoretical prediction on the distribution of the captured particles. The most probable principal quantum number of the initially formed state is estimated to be $n = \sqrt{M^*/m_e} \simeq 38$, where M^* is the reduced mass of the captured antiproton and m_e is the electronic mass. The total angular momentum J of this state is expected to be equal to the angular momentum of the corresponding circular orbit, i.e., $J = l = n - 1$. In this communication we shall derive a semianalytic wave function for metastable states of $\bar{p}He^+$ which has all symmetry properties of the state and its kinematical features exactly incorporated. They define the probability distribution and, as a result, the physical characteristics of the state. Though a pseudosymmetry operator, accounting for the above-mentioned kinematic features of metastable states can be formally created, we just consider them as forming «the character» of the state [5,6]. In a similar context, propensity rules for radiative and non-radiative decay of resonant states of two-electron atoms, also of the positronium negative ion [7], based on the underlying approximate molecular-orbital structure, demonstrate the usefulness of the idea.

Let $\mathbf{X}$ and $\mathbf{x}$ be Jacobi vectors for the three-body system $\bar{p} + e + \alpha$ (see the Figure). It is a standard molecular configuration but contrary to the usual case the mass of the «valence» particle is the biggest. The hyperradius R and the corresponding reduced masses M and μ are given by

$$MR^2 = MX^2 + \mu x^2$$

$$\frac{1}{M} = \frac{1}{m_{\bar{p}}} + \frac{1}{m_e}, \quad \frac{1}{\mu} = \frac{1}{m_\alpha} + \frac{1}{m_{\bar{p}} + m_e}. \tag{1}$$

The total centre of mass Hamiltonian of the problem then reads

$$H = -\frac{1}{2M}\frac{1}{R^5}\frac{\partial}{\partial R}R^5\frac{\partial}{\partial R} + \frac{\Lambda^2}{2MR^2}, \tag{2}$$

depending on the set of six coordinates $\{R, \hat{o}\}$, where $\hat{o}$ serves for five hyperspherical angles. The most commonly used space-fixed choice of variables $\hat{o}$ is $\{\alpha_c, \hat{\mathbf{x}}, \hat{\mathbf{X}}\}$ with $\hat{\mathbf{x}}$ and $\hat{\mathbf{X}}$ defining the polar angles of the corresponding vectors and

$$\alpha_c = \arctan\left(\frac{\sqrt{M}X}{\sqrt{\mu}x}\right). \tag{3}$$

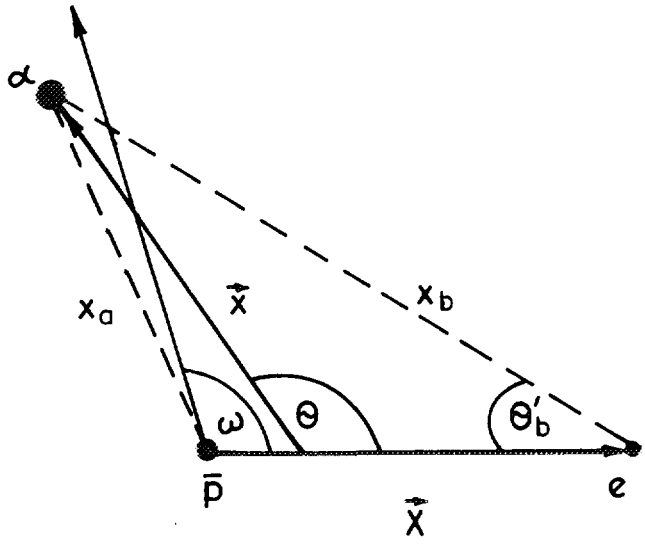

Figure. Three-body molecular Jacobi coordinates **X** and **x** (*c*-set), with α-particle playing the role of the valence particle, form the reference configuration [$\tan(2\omega) = \mu x^2 \sin(2\theta)/(MX^2 + \mu x^2 \cos(2\theta))$]. As α-particle and $\bar{p}$ are much more heavier than electron, the actual position of **x** and the inertial tensor principal axis cannot be pictured properly, they practically coincide with x_a and $\omega \approx \theta_a'$. Two additional Jacobi-vector sets (*a* and *b*) are not pictured. They are defined as in our paper [8]

In this case

$$\Lambda^2 = -\frac{1}{\sin^2 2\alpha_c}\frac{\partial}{\partial\alpha_c}\sin^2 2\alpha_c \frac{\partial}{\partial\alpha_c} + \frac{\mathbf{l}^2}{\cos^2\alpha_c} + \frac{\mathbf{L}^2}{\sin^2\alpha_c}, \tag{4}$$

where **l** and **L** are the angular momenta corresponding to **x** and **X**. As is well known there are three different sets of Jacobi vectors for a three-body problem so the underscript notifies the set chosen.

The hyperspherical harmonics (HH) are defined as the solutions of the angular part of the Schrödinger equation

$$[\Lambda^2 - K(K+4)]Y_K(\hat{o}) = 0, \tag{5}$$

with K being the quantum number of the so-called grand angular momentum. As only normal parity states, i.e., those for which the quantum number of the total parity $p = (-)^J$, will be considered in the communication, we can omit the superscript in the corresponding context.

The recently derived parametrization of the body-frame HH [8] will be intensively used in our derivation. It reads

$$\mathbf{Y}^{JpM_J}_{KlL(c)}(\xi, \eta, \gamma, \beta, \tilde{\alpha}) = \sum_{m'=0(1)}^{J} y^{Jp}_{KlLm'(c)}(\xi, \eta) B^{JpM_J}_{m'}(\gamma, \beta, \tilde{\alpha}), \tag{6}$$

where

$$y^{Jp}_{KlLm'(c)}(\xi, \eta) = f_{KlL}(\alpha_c) \sum_{m}^{J} P^m_l(\theta) d^{Jp}_{m,m'}(\omega) U^{Jpl}_{mL}, \tag{7}$$

$$B^{JpM_J}_m(\gamma, \beta, \tilde{\alpha}) = \frac{(-i)^m}{4\pi} \sqrt{\frac{2J+1}{1+\delta_{0m}}} [D^J_{-m,-M_J}(\gamma, \beta, \tilde{\alpha}) + p(-)^J D^J_{m,-M_J}(\gamma, \beta, \tilde{\alpha})] \tag{8}$$

with the coefficients forming the Clang-Fano orthogonal matrix [9]

$$U^{Jpl}_{mL} = p(-)^{J+l+m} \sqrt{2-\delta_{0m}} (l, J, -m, m \,|\, L, 0). \tag{9}$$

$P^m_l(\theta)$ are the normalized associated Legendre polynomials of cos θ and the parity projected combination of the Rose d-functions [10] is of the form

$$d^{Jp}_{m,m'}(\omega) = \frac{1}{\sqrt{(1+\delta_{0m})(1+\delta_{0m'})}} [d^J_{m,m'}(\omega) + p(-)^{J+m'} d^J_{m,-m'}(\omega)] \,. \tag{10}$$

As is indicated in (7) all three auxiliary variables α_c, cos θ, ω should be expressed in terms of common dynamic variables {ξ, η}, say, hyperspheroidal coordinates [8]. The parameter ω defines the angle between the vector **X** and the principal axis of the three-body inertia-tensor (Figure). The {γ, β, $\tilde{\alpha}$}-set is given by the Euler rotation bringing the space-fixed frame into the inertia-tensor frame. Following [11] we shall choose among solutions (6) the HH which do not have internal (configurational) excitation by putting

$$K = J = l + L. \tag{11}$$

Under this condition we have

$$f_{KlL}(\alpha_c) = \cos^l \alpha_c \sin^L \alpha_c \tag{12}$$

thus finishing the specification of the three-body angular basis (6).

By introducing the partial-wave expansion of HH into the eigenvalue equation (5) and integrating over {γ, β, $\tilde{\alpha}$}-variables we arrive at the system of $J+1$ Schrödinger equations for vector-column HH (7) with the components $m' = 0, 1, \ldots, J$ defining the projection of the total angular momentum onto the body-fixed z-axis.

Now we are ready to construct the wave-function for $\bar{p}\mathrm{He}^+$ metastable states. They should be molecular orbitals formed by two approximately degenerate atomic orbitals: $(\alpha + e)$-hydrogenic state depending on radial variable x_b, with principal quantum number $n_b = 1$, and $(\alpha + \bar{p})$-hydrogenic state depending on $\mathbf{x}_a$ with $n_a = J + 1$, angular momentum $L_{\mathbf{x}_a} = J$.

Firstly, we note that due to specific mass relations for the particles constituting $\bar{p}\mathrm{He}^+$ we have $\omega \simeq \theta_a'$ (Fig.), and the quantization axis practically coincides with the corresponding side of the particle triangle. Thus, as the electron is occupying the ls-state the total angular momentum J is mainly due to the pair angular motion given by $L_{\mathbf{x}_a}$ and,

as a result, only ($m' = 0$)-component of the wave-function survives. Accordingly, the molecular orbital of the metastable state can be written in the form

$$\varphi(R, \xi, \eta, \tilde{\alpha}, \beta, \gamma) = B_0^J(\gamma, \beta, \tilde{\alpha}) R^J [\tilde{c}_1(R) f_{JOJ}(\alpha_a) d_{0,0}^{Jp}(\omega_a) U_{0J}^{Jp0} e^{-\sqrt{-\epsilon_n} x_a} +$$

$$+ \tilde{c}_2(R) f_{JJ0}(\alpha_b) \sum_m P_J^m(\theta_b) d_{m,0}^{Jp}(\omega_b) U_{m0}^{JpJ} e^{-\sqrt{-\epsilon_1} x_b}], \tag{13}$$

where we have used the functional form (7) twice with

$$\tan \alpha_a = \frac{\sqrt{\mu_a} x_a}{\sqrt{M_a} X_a}, \quad \cos \theta_a = \hat{\mathbf{x}}_a \cdot \hat{\mathbf{X}}_a, \quad \omega_a = \theta_a' - \omega \text{ (Fig.)}, \tag{14}$$

and where the reduced masses μ_a and M_a correspond to Jacobi vectors $\mathbf{x}_a$ and $\mathbf{X}_a$, respectively; similar notation holds for the Jacobi pair $\mathbf{x}_b$ and $\mathbf{X}_b$. Naturally, ε_n and ε_1 are the energies of the corresponding orbitals or variational parameters close to their values. The particular form (13) demonstrates the flexibility of the parametrization of HH in the form (7): starting from the space-fixed frame we were able to factorize γ, β, $\tilde{\alpha}$-Euler rotation as

$$\hat{D}^{Jp}(\gamma, \beta, \tilde{\alpha}) = \hat{D}^{Jp}(0, \omega_a, 0) \hat{D}^{Jp}(\phi_a, \hat{\mathbf{x}}_a) \tag{15}$$

for the antiprotonic orbital and as

$$\hat{D}^{Jp}(\gamma, \beta, \tilde{\alpha}) = \hat{D}^{Jp}(0, \omega_b, 0) \hat{D}^{Jp}(\phi_b, \hat{\mathbf{x}}_b) \tag{16}$$

for the electronic state, where $\hat{D}^{Jp}(0, \omega, 0)$ is the parity-preserving rotation in the triangle plane and $\phi_{a(b)}$ is the azimuthal angle of the corresponding vectors.

The general expression for $y^J_{KlLm'}$ (7) can be further simplified for both $y^J_{J0J0(a)}$ and $y^J_{JJ00(b)}$ if we make use of the following expressions

$$U_{m0}^{JpJ} = p(-)^{J+m} \sqrt{2 - \delta_{0m}} \frac{1}{\sqrt{2J+1}}$$

$$P_J^m(\theta) = (-)^m \frac{\sqrt{(2J+1)(1+\delta_{0m})}}{2} d_{0m}^{Jp}(\theta) \tag{17}$$

and apply the group property of $\mathbf{d}^{Jp}$-matrices [11]

$$d_{mm'}^{Jp}(\alpha + \beta) = \sum_{\mu=0}^{J} d_{m\mu}^{Jp}(\alpha) d_{\mu m'}^{Jp}(\beta). \tag{18}$$

The simplified form of (13) will then be

$$\psi(\text{Atomcule}) = [c_1(R) x_a^J e^{-\sqrt{-\epsilon_n} x_a} P_J(\omega_a) +$$

$$+ c_2(R) X_b^J e^{-\sqrt{-\epsilon_1} x_b} P_J(\omega_b - \theta_b)] B_0^J(\gamma, \beta, \tilde{\alpha}). \tag{19}$$

Here the $\sin^J\alpha$ factor supplied by the scalar part (12) of the HH (7) has been used to account exactly for the pair-interaction singularity. Though $\omega_a \simeq 0$ and $\omega_b \simeq \theta_b$ hold, the

Legendre polynomials $P_j(\omega_a)$ and $P_J(\omega_b - \theta_b)$ provide the correlation due to electron-antiproton interaction and play the crucial kinematic role incorporating the two-body relative motion into the three-body wave function.

«The character» of the long-lived antiprotonic states is emphasized by the primitive form of their wave function (19). Accordingly, these states comprise a specific series of resonant states with its own «ground state». As the probability distribution for the states (19) is of some particular configuration one might expect the overlap integral between them and non-molecular states to be small. The approximate solution (19) is keeping equal to zero the projection of the total angular momentum onto the body-fixed z-axis. One more approximate quantum number specifying «the character» of the metastable state will appear if we introduce the hyperradial-adiabatic approximation [12,13]: it will be the vibrational quantum number describing the excitation mode in the corresponding adiabatic potential.

To finish the paper we answer the question: «What metastable antiprotonic states are: atomic or molecular states?» They are definitely molecular states as they exist due to the peculiar correlation between the electron and antiproton motion and they are long-lived just because of their molecular form (19). On the other hand, crude energetic characteristics of the metastable states can be calculated in a kinematically more primitive approaches: keeping either α-particle (atomic picture) or both, α-particle and antiproton (Born-Oppenheimer adiabatic description), fixed.

The title of the recent paper by J.M.Rost and D.Wintgen [7] is: «Positronium Negative Ion: Molecule or Atom?» Using hyperspherical adiabatic approach they demonstrate the molecular mode in the resonance spectrum of $(e + e + e^+)$-system that is, of course, not so much evident for the ground state of the system.

References

1. Morita N. et al. — Phys. Rev. Lett., 1994, v.72, p.1180; Maas F. et al. — Phys. Rev., 1995, v.A52, p.4266.
2. Condo G.T. — Phys. Lett., 1964, v.9, p.65.
3. Russel J.E. — Phys. Rev. Lett., 1969, v.23, p.63; Phys. Rev., 1969, v.188, p.187; Phys. Rev., 1970, v.A1, p.721; Phys. Rev., 1970, v.A1, p.735; Phys. Rev., 1969, v.A1, p.742.
4. Korobov V.I. — Phys. Rev., 1996, v.A54, p.R1749.
5. Russek A., Furlan R. — Phys. Rev., 1989, v.A39, p.5034.
6. Riera A. — In: Time Dependent Molecular Dynamics, Plenum Press, New York, 1992.
7. Rost J.M. — Hyperfine Int., 1994, vol.89, p.343; Rost J.M., Wintgen D. — Phys. Rev. Lett., 1992, v.69, p.2499.
8. Matveenko A.V., Fukuda H. — J. Phys., 1996, v.B29, p.1575.
9. Chang E.S., Fano U. — Phys. Rev., 1972, v.A6, p.173.
10. Rose M.E. — Elementary Theory of Angular Momentum, New York: Wiley, 1957.
11. Matveenko A.V., Fukuda H. — to be published.
12. Macek J.H. — J. Phys., 1968, v.B1, p.831.
13. Matveenko A.V. — Phys. Lett., 1985, v.B129, p.11.

Received on October 15, 1996.

XJ9700065

УДК 539.12.01 + 539.12.125

NEXT-TO-NEXT-TO-LEADING ORDER QCD ANALYSIS OF COMBINED DATA FOR xF_3 STRUCTURE FUNCTION AND HIGHER-TWIST CONTRIBUTION

A.V.Sidorov

The simultaneous QCD analysis of the xF_3 structure function measured in deep-inelastic scattering by several collaborations is done up to 3-loop order of QCD. The x dependence of the higher-twist contribution is evaluated and turns out to be in a qualitative agreement with the results of «old» CCFR data analysis and with renormalon approach predictions. The Gross–Llewellyn Smith sum rule and its higher-twist corrections are evaluated.

The investigation has been performed at the Bogoliubov Laboratory of Theoretical Physics, JINR.

Совместный КХД анализ данных по xF_3 в третьем порядке теории возмущений и определение вклада высших твистов

А.В.Сидоров

Совместный КХД анализ данных по структурной функции xF_3, измеренной различными коллаборациями, проведен в 1-, 2- и 3-петлевом приближении. Определена x-зависимость вклада высших твистов в структурную функцию. Определена экспериментальная величина вклада высших твистов в правило сумм Гросса – Льювеллина-Смита.

Работа выполнена в Лаборатории теоретической физики им. Н.Н.Боголюбова ОИЯИ.

1. The experimental data of the CCFR collaboration (we'll call them «old») obtained at Fermilab Tevatron [1] for the xF_3 structure functions of deep-inelastic scattering of neutrinos and antineutrinos on an iron target provide an important means of accurate comparison of QCD with experiment. However, in view of revision of «old» data announced by CCFR collaboration [2] the question arises: what can we say about the comparison of the QCD predictions on Q^2 dependence of the $xF_3(x, Q^2)$ structure function (SF) based on the data of neutrino DIS experiments different from those of CCFR?

In the present note, a combined fit of the experimental data of the CDHS [3], SCAT [4], BEBC-WA59 [5], BEBC-Gargamelle [6] and JINR-IHEP [7] collaborations for the xF_3 structure functions is done in order to determine the x dependence of the SF, higher twist (HT) contribution and the value of the scale parameter $\Lambda_{\overline{MS}}$.

2. We'll use, for the QCD analysis, the Jacobi polynomial expansion method proposed in [8]. It was developed in [8]—[14] and applied for the 3-loop order of peturbative QCD (pQCD) to fit F_2 [13] and xF_3 data [14,15].

The Q^2-evolution of the moments $M_3^{pQCD}(N, Q^2)$ is given by the well-known perturbative QCD [16,17] formula:

$$M_3^{pQCD}(N,Q^2) = \left[\frac{\alpha_S(Q_0^2)}{\alpha_S(Q^2)}\right]^{d_N} H_N(Q_0^2,Q^2) M_3^{pQCD}(N,Q_0^2), \quad N = 2, 3, \ldots$$
$$d_N = \gamma^{(0),N}/2\beta_0. \tag{1}$$

The factor $H_N(Q_0^2,Q^2)$ contains next- and next-to-leading order QCD corrections* and is constructed in accordance with [14] based on theoretical results of [19].

The expression (1) provides an input for reconstruction of the SF by the Jacobi polynomial method. Following the method [10,11], we can write the leading twist contribution to the structure function xF_3 in the form:

$$xF_3^{pQCD}(x,Q^2) = x^\alpha(1-x)^\beta \sum_{n=0}^{N_{max}} \Theta_n^{\alpha\ \beta}(x) \sum_{j=0}^{x} c_j^{(n)}(\alpha,\beta)(\beta) M_3^{QCD}(j+2, Q^2), \tag{2}$$

where $\Theta_n^{\alpha\beta}(x)$ is a set of Jacobi polynomials and $c_j^{(n)}(\alpha, \beta)$ are coefficients of the series of $\Theta_n^{\alpha\beta}(x)$ in powers of x:

$$\Theta_n^{\alpha\beta}(x) = \sum_{j=0}^{n} c_j^{(n)}(\alpha, \beta)(\beta) x^j. \tag{3}$$

The unknown coefficients $M_3(N, Q_0^2)$ in (1) could be parametrized as Mellin moments of some function:

$$M_3^{pQCD}(N, Q_0^2) = \int_0^1 dx x^{N-2} A x^b (1-x)^c (1+\gamma x), \quad N = 2, 3, \ldots \tag{4}$$

To extract the HT contribution, the nonsinglet SF is parametrized as follows:

$$xF_3(x,Q^2) = xF_3^{pQCD}(x, Q^2) + h(x)/Q^2, \tag{5}$$

where the Q^2 dependence of the first term in the r.h.s. is determined by perturbative QCD. Constants $h(x_i)$ (one per x-bin) parameterize the HT x dependence. We put x_i = 0.03, 0.05, 0.08, 0.15, 0.25, 0.35, 0.45, 0.50, 0.55, 0.65, 0.80 for i = 1, 2... 11. The HT contribution or F_2 was determined in [20]. The values of constants $h(x_i)$ as well as the parameters A, b, c, γ and scale parameter Λ are determined by fitting the combined set of data of 192 experimental points of xF_3 in a wide kinematic region: 0.5 GeV$^2 \le Q^2 \le$ 196 GeV^2 and $0.03 \le x \le 0.80$ and Q_0^2 = 10 GeV^2. We have put the number of flavors to equal 4. In accordance with the result of [3] concerning the disagreement of their data with perturbative QCD at small x, a cut $x \ge 0.35$

*For reviews and references on higher order QCD results see [18].

Table. Results of the 1-, 2- ($N_{max} = 10$) and 3- order ($N_{max} = 8$) QCD fit (with TMC) of the combined xF_3 SF data for $f = 4$, $Q^2 > 0.5$ GeV^2 with the corresponding statistical errors, normalization coefficients and values of the HT contribution $h(x_i)$

	1-loop approx.	2-loop approx.	3-loop approx.
$\chi^2_{d.f.}$	312/176	316/176	312/176
A	6.68 ± 0.38	6.92 ± 1.43	7.11 ± 0.38
b	0.760 ± 0.027	0.768 ± 0.072	0.778 ± 0.027
c	4.03 ± 0.07	3.97 ± 0.17	3.82 ± 0.07
γ	0.675 ± 0.156	0.452 ± 0.624	0.189 ± 0.128
$\Lambda_{\overline{MS}}$, MeV	191 ± 46	159 ± 39	163 ± 31
x_i		$h(x_i)$, GeV^2	
0.03	0.086 ± 0.087	0.090 ± 0.091	0.067 ± 0.085
0.05	0.001 ± 0.028	0.022 ± 0.032	0.093 ± 0.047
0.08	-0.127 ± 0.123	-0.094 ± 0.126	-0.011 ± 0.131
0.15	-0.286 ± 0.046	-0.230 ± 0.050	-0.200 ± 0.050
0.25	-0.401 ± 0.058	-0.334 ± 0.056	-0.327 ± 0.054
0.35	-0.284 ± 0.073	-0.220 ± 0.068	-0.178 ± 0.062
0.45	-0.436 ± 0.093	-0.366 ± 0.090	-0.403 ± 0.083
0.50	0.005 ± 0.079	0.047 ± 0.077	0.036 ± 0.074
0.55	-0.243 ± 0.069	-0.200 ± 0.068	-0.242 ± 0.064
0.65	0.176 ± 0.063	0.202 ± 0.072	0.154 ± 0.060
0.80	0.020 ± 0.037	0.024 ± 0.039	-0.012 ± 0.039

was used for CDHS data. The target mass corrections (TMC) are taken into account to the order $o(M^4_{nucl}/Q^4)$ [14].

The nuclear effect of the relativistic Fermi motion is estimated from below by the ratio $R_F^{D/N} = F_3^D/F_3^N$ obtained in the covariant approach in light-cone variables [21].

3. Results of the fit for distribution parameters, the shape of the next twist contribution $h(x)$ and parameter Λ are presented in the Table and in the Figure.

The experimental values of xF_3 for each collaboration were multiplied by the normalization factors C^{coll} which were considered as free parameters. Their values are not sensitive to the order of pQCD in use and were found to be equal to: $C^{BEBC-WA59} = 0.92 \pm 0.03$, $C^{SCAT} = 1.06 \pm 0.03$, $C^{JINR-IHEP} = 1.02 \pm 0.05$, and $C^{BEBC-Gard} = 0.97 \pm 0.04$. The value of $C^{CDHS} = 1$ was fixed.

The obtained value of $\Lambda_{\overline{MS}}$ is larger than that given by a similar analysis of CCFR data [15] $\Lambda_{\overline{MS}} = 134 \pm 57$ MeV but exhibits relatively small statistical errors. Results of the NLO and NNLO fit the constant of strong interaction $\alpha_S^{NLO}(M_Z^2) = 0.105 \pm 0.004$ and $\alpha_S^{NNLO}(M_Z^2) = 0.107 \pm 0.003$ in agreement, within the errors, with usual DIS results [22]. Additional uncertainties to the value of $\alpha_S(M_Z^2)$ due to extrapolation of the Q^2 dependence of the SF with four flavors ($f = 4$) in a wide kinematic interval $0.5\ \text{GeV}^2 \le Q^2 \le 196\ \text{GeV}^2$ were found to be about 0.001 in [23] and 0.5 should be taken into account, too.

The value of the perturbative part of the GLS sum rule [24] at $Q^2 = 10\ \text{GeV}^2$ estimated by using results of the Table is equal to $\int_0^{-1} \frac{xF_3^{pQCD}(x)}{x}\,dx = 2.60 \pm 0.23$ in agreement with results of the «old» CCFR data analysis [25,12].

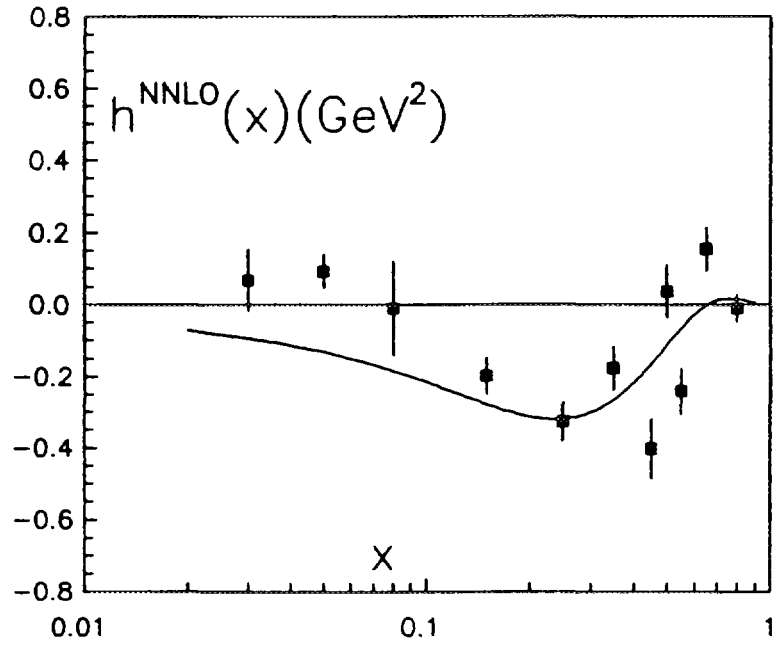

Figure. Higher-twist contributions from NNLO$_s$ fit and the theoretical prediction for $h(x)$ from [26]

The shape of $h(x)$ is in qualitative agreement with theoretical predictions of the dispersion method of the renormalon approach [26] (for reviews and references see [27]) and with results of the QCD analysis of «old» CCFR data presented in [15]. The only difference is the positive value of measured $h(x)$ at small x. The obtained $h(x)$ obviously differs from the precise values of HT contribution for singlet SF F_2 presented in [20]. See also [28] for model dependent evolution of $h(x)$.

4. In conclusion it should be stressed that combined fit provides still a more precise determination of $\Lambda_{\overline{MS}}$ and $h(x_i)$ in comparison to the analysis of «old» CCFR data [15], while the shape of the SF ruled by parameters A, b, c and γ is determined less accurate. The most discrepancy with the «old» CCFR data analysis takes place for the HT contribution to the GLS sum rule and for the HT x dependence at large x.

Based on the results of the Table, one can estimate the value of the first moment of $h(x)$: $h_1 = \int_0^1 \frac{h(x)}{x}\,dx$. The obtained values: $h_1^{\rm LO} = -0.42 \pm 0.27^*$, $h_1^{\rm NLO} = -0.29 \pm 0.28$, and $h_1^{\rm NNLO} = -0.26 \pm 0.27$ are in agreement with theoretical predictions of [29] $h_1 = -0.29 \pm 0.14$ and [30] $h_1 = -0.47 \pm 0.04$ as well as with the recent result of [31].

For a more precise determination of the HT contribution to SF, the role of the nuclear effect should be clarified and a more realistic approximation for $R_F^{\rm Fe/N} = F_3^{\rm Fe}/F_3^{\rm N}$ is needed. We also did not take into account the threshold effects on Q^2 evolution of SF due to heavy quarks [32] which is necessary owing to a wide kinematic region of data under consideration and have been realized in [23].

Acknowledgements

The author is grateful to S.A.Bunyatov, A.L.Kataev, V.G.Krivokhizhin, S.A.Larin, S.V.Mikhailov, and M.V.Tokarev for discussions. This investigation has been supported in part by INTAS grant No.93-1180 and by the Russian Foundation for Fundamental Research (RFFR), No.95-02-04314a.

References

1. CCFR Collab. Quintas P.Z. et al. — Phys. Rev. Lett., 1993, v.71, p.1307;
   CCFR Collab. Shaevitz M. et al. — Nucl. Phys. Proc. Suppl, 1995, v.B38, p.188.
2. CCFR/NuTeV Collab. Harris D. — Talk at the XXVIII Int. Conf. on HEP, Warsaw, July 1996;
   Spntzouris P. — Talk at the DPF Meeting of APS, Minnesota, August 1996.
3. Berge P. et al. — Z.Phys., 1991, v.C49, p.187.
4. SKAT Collab. Ammosov V.V. et al. — Z. Phys., 1986, v.C30, p.175.
5. BEBC-WA59 Collab. Varvell K. et al. — Z.Phys., 1987, v.C36, p.1.
6. Bosetti P.C. et al. — Nucl. Phys., 1982, v.B203, p.362.
7. JINR-IHEP Collab. Barabash L.S. et al. — JINR, E1-96-308, Dubna, 1996, [hep-ex/9611012].
8. Parisi G., Sourlas N. — Nucl. Phys., 1979, v.B151, p.421;
   Barker I.S., Langensiepen C.B., Shaw G. — Nucl. Phys., 1981, v.B186, p.61.

*Hereafter present the value of $h(x)$ in [GeV^2].

9. Barker I.S., Martin B.R., Shaw G. — Z. Phys., 1983, v.C19, p.147;
Barker I.S., Martin B.R. — Z.Phys., 1984, v.C24, p.255.
10. Krivokhizhin V.G. et al. — Z.Phys., 1987, v.C36, p.51; Z.Phys., 1990, v.C48, p.347.
11. BCDMS Collab. Benvenuti A. et al. — Phys. Lett., 1987, v.B195, p.97; 1989, v.B233, p.490.
12. Kataev A.L., Sidorov A.V. — Phys. Lett., 1994, v.B331, p.179.
13. Parente G., Kotikov A.V., Krivokhizhin V.G. — Phys. Lett., 1994, v.B333, p.190.
14. Kataev A.L., Kotikov A.V., Parente G., Sidorov A.V. — Phys. Lett., 1996, v.B388, p.179.
15. Sidorov A.V. — JINR, E2-96-254, Dubna, 1996 [hep-ph/9607275], to be published in Phys. Lett.B.
16. Yndurain F.J. — Quantum Chromodynamics (An Introduction to the Theory of Quarks and Gluons), Berlin, Springer-Verlag, 1983.
17. Buras A. — Rev. Mod. Phys., 1980, v.52, p.199.
18. Van Neerven W.L. — To appear in the Proceedings of the 1996 HERA Physics workshop, [hep-ph/9609243].
19. Van Neerven W.L., Zijlstra E.B. — Phys. Lett. 1991, v.272B, p.127; 1991, v.273B, p.476; Nucl. Phys., 1992, v.B383, p.525;
Zijkstra E.B., van Neerven W.L. — Phys. Lett., 1992, v.297B, p.388; Nucl. Phys., 1994, v.B417, p.61;
Larin S.A., van Ritbergen T., Vermaseren J.A.M. — Nucl. Phys., 1994, v.B427, p.41;
Tarasov O.V., Vladimirov A.A., Zharkov A.Yu. — Phys. Lett., 1980, v.B93, p.429.
20. Virchaux M., Milsztajn A. — Phys. Lett., 1992, v.B274, p.221.
21. Braun M.A., Tokarev M.V. — Phys. Lett., 1994, v.B320, p.381;
Tokarev M.V. — Phys. Lett., 1993, v.B318, p.559;
Sidorov A.V., Tokarev M.V. — Phys. Lett., 1995, v.B358, p.353.
22. Bethke S. — Nucl. Phys. (Proc. Suppl.), 1995, v.39B,C, p.198.
23. Shirkov D.V., Mikhailov S.V., Sidorov A.V. — JINR, E2-96-285, Dubna, 1996 [hep-ph/9607472].
24. Gross D.J., Llewellyn-Smith C.H. — Nucl. Phys., 1969, v.B14, p.337.
25. CCFR Collab., Leung W.C. et al. — Phys. Lett., 1993, v.B317, p.655.
26. Dasgupta M., Webber B.R. — Cavendish-HEP-96/1 [hep-ph/9604388].
27. Zakharov V.I. — Nucl. Phys., 1992, v.B385, p.452;
Mueller A.H. — In: QCD 20 Yars Later, v.1, World Scientific, Singapore, 1993;
Webber B.R. — Cavendish-HEP-96/2 [hep-ph/9604388], talk at DIS96, Rome, April 1996.
28. Bednyakov V.A. et al. — Sov.J.Yad.Fiz., 1984, v.40, p.770.
29. Braun V.M., Kolesnichenko A.V. — Nucl. Phys., 1987, v.B283, p.723.
30. Ross G.G., Roberts R.G. — Phys. Lett., 1994, v.B322, p.425.
31. Balitsky I.I., Braun V.M., Kolesnichenko A.V. — Phys. Lett., 1990, v.B242, p.245; (E) ibid, 1993, v.B318, p.648;
Braun V.M. — [hep-ph/9505317], to appear in the Proceedings of the XXXth Rencontres de Moriond «QCD and High Energy Hadronic Interactions» Les Ars, France, March 1995.
32. Bernreuther W., Wetzel W. — Nucl. Phys., v.B197, p.228;
Marciano W. — Phys. Rev., 1984, v.D29, p.580;
Shirkov D.V. — Nucl. Phys., 1992, v.B371, p.267;
Shirkov D.V., Mikhailov S.V. — Z.Phys., 1994, v.C63, p.463.

Received on November 19, 1996.

XJ9700066

УДК 621.039: 621.384.6

МОЩНЫЕ ПУЧКИ НЕЙТРОНОВ С ИСПОЛЬЗОВАНИЕМ УСКОРИТЕЛЕЙ

В.Н.Михайлов*

Рассмотрены возможности использования в ядерной энергетике мощных пучков нейтронов, создаваемых ускоренными заряженными частицами, основные требования к пучку таких частиц и к ускорителю.

Powerful Neutron Beams from Accelerators

V.N.Mikhailov

A possibility of using powerful beams from particle accelerator in nuclear engineering and basic requirements to beam parameters as well as the accelerator type have been discussed.

Введение

Возможности использования в ядерной энергетике нейтронных потоков, образуемых пучками заряженных частиц из ускорителя, обсуждаются учеными с конца 40-х годов (подробности можно найти в [1]). Под действием ускоренных протонов или других частиц в мишени из свинца или висмута образуется 20 + 25 быстрых нейтронов, которые затем термализуются и размножаются в окружающей оболочке, представляющей собой подкритический реактор на тепловых нейтронах. Такую схему сейчас называют усилителем энергии [2], и она имеет как своих сторонников, так и противников.

Сторонники электроядерного метода подчеркивают такие его преимущества, как способность сжигать ^{232}Th или обедненный уран, более короткий по сравнению с реакторами на быстрых нейтронах цикл наработки делящихся материалов, наконец, его повышенную безопасность, исключающую вероятность возникновения в реакторе неуправляемой цепной реакции (НЦР), а в случае ториевого цикла — также и возможность неконтролируемого распространения ядерного оружия.

Напротив, оппоненты подчеркивают низкую эффективность ускорителей, приводящую к высоким затратам энергии на один полученный в такой установке нейтрон, недостаточную интенсивность ускоренного пучка и высокие начальные капиталовло-

* Министерство атомной промышленности России, Москва

жения. При этом они исходили из спорного положения, что «то обстоятельство, что в подкритическом реакторе в отличие от критического не может осуществляться НЦР, не является серьезным аргументом в пользу ускорительного метода. Многолетняя практика показала, что регулировать самоподдерживающуюся реакцию и защищать реактор от НЦР нетрудно» [3].

Можно согласиться с тем, что «нетрудно защитить реактор от НЦР», но очень трудно и крайне дорого, как показал опыт Чернобыля, устранять последствия ее возникновения, поэтому полное исключение возможной НЦР представляется делом, оправдывающим увеличение начальной стоимости электроядерного реактора.

Действительно, сегодня нет действующего ускорителя, способного поставлять пучок протонов мощностью порядка 100 МВт и отвечающего всем другим требованиям. Это в первую очередь связано с тем, что ускорители развивались для нужд экспериментальной физики, где такие уровни мощности не нужны. И хотя на импульсных ускорителях мгновенная мощность пучков, например, электронов лежит в диапазоне ГВт, средняя мощность ускоренных пучков остается на уровне десятков киловатт.

Вместе с тем непрерывное развитие технологии ускорителей, особенно в последние 10—15 лет, и техники получения и управления пучками достаточной интенсивности позволяет по-новому взглянуть на задачу создания нейтронного пучка, отвечающего требованиям электроядерного реактора. В этой работе кратко рассмотрим основные требования к пучку быстрых частиц, генерирующему их ускорителю и возможные направления его реализации.

Требования к пучку быстрых частиц

В общем виде электроядерный реактор работает по следующей схеме.

Рабочее вещество реактора таково, что число рождающихся нейтронов меньше числа первичных, и реакция деления быстро затухает, если для ее поддержания в активную зону реактора не поставляются нейтроны от внешнего источника. Таким источником может быть ускоритель протонов или других частиц достаточно высокой энергии, которые при взаимодействии с мишенью из тяжелых элементов дают первичный поток нейтронов высокой энергии. Нейтронный поток из мишени попадает в размножающую оболочку, где термализуется, и реакция деления идет на тепловых нейтронах. В таком подкритическом реакторе его мощность всегда пропорциональна мощности пучка поступающих от ускорителя частиц, т.е. реактор оказывается лишь своеобразным усилителем энергии пучка ускорителя.

Если ускоритель поставляет пучок протонов мощностью пучка P_b, то в реакторе выделяется тепло мощностью $P_h = GP_b$, где G — коэффициент «усиления» мощности пучка. Тогда полезная мощность электроядерного реактора P_u равна

$$P_u = (G\eta_e - 1/\eta_g\eta_b)P_b - P_a. \qquad (1)$$

Здесь P_a — мощность собственных нужд ускорителя, расходуемая на его поддержание в рабочем состоянии независимо от мощности пучка, η_e — кпд преобразования элект-

ростанцией тепловой энергии в электрическую, η_g — кпд преобразования мощности промышленной частоты в высокочастотную, η_b — кпд передачи ВЧ-мощности ускоряемому пучку.

В этом выражении ряд параметров имеет проверенную на практике величину. Так, величина η_e на действующих электростанциях равна 0,35. Коэффициент η_g зависит от типа ВЧ-генератора и его рабочей частоты, и в рассматриваемых ниже ускорителях может быть принят равным 0,6. Коэффициент η_b определяется типом ускорителя, и его можно подожить равным 0,9.

Величина G определяется многими параметрами: видом и энергией быстрых заряженных частиц (протоны или более тяжелые [4]), материалом мишени, размножающей оболочки и других конструкций реактора. Надо отметить, что точные данные по физике процессов в электроядерном реакторе отсутствуют. Имеющиеся экспериментальные данные получены на различных упрощенных моделях мишеней и подлежат систематизации и дополнительной проверке, т.к. их точность не превосходит 20 + 30%. По оптимистическим предположениям [2] для протонов с энергией 1 ГэВ усиление G может достигать в реакторе величины 30 + 35. Если подставить эти величины в (1), то получим

$$P_u = (10{,}5 - 1{,}85)P_b - P_a . \qquad (2)$$

Полагая, что мощность собственных нужд ускорителя P_a составляет 1 + 3 МВт и для оценок ею можно пренебречь, из (2) находим, что рассматриваемый реактор способен производить электроэнергию мощностью порядка 1 ГВт, а именно такой мощности реактор имеет промышленное значение, если мощность пучка протонов 100 + 120 МВт. Следовательно, интенсивность пучка протонов должна быть 0,1 А и выше.

Эту мощность следует распределить в мишени по некоторому объему с тем, чтобы исключить ее нагрев выше достижимого удельного теплосъема, а также получить возможно более равномерное поле нейтронов в рабочей зоне. Для этого достаточно, по-видимому, разделить протонный пучок на 10 + 15 пучков меньшей интенсивности и облучать несколько мишеней в центре реактора. Материалом мишени может быть свинцово-висмутовый расплав, одновременно выполняющий роль теплоносителя первичного контура охлаждения. При разделении пучка протонов снижаются также требования к «выпускному окну» ускорителя.

Разумеется, ускорение пучка должно сопровождаться минимальными потерями, а управление им быть практически безынерционным.

Тип ускорителя

Выбор типа ускорителя в первую очередь определяется надежностью и эксплуатационными качествами (эффективность, стоимость, долговечность, ремонтоспособность и др.) ВЧ-преобразователя. Следует также учитывать опыт, полученный в 70-х годах при сооружении мезонных фабрик. Тогда в США был построен линейный ускоритель в Лос-Аламосе [5], в Канаде — циклотрон «Triumf» в Ванкувере [6], в

Европе — циклотрон SIN в Цюрихе [7], а позже у нас — линейный ускоритель в Троицке [8]. Хотя на этих ускорителях энергия пучка в 1,5-2 раза и интенсивность в 100 раз меньше требуемой, тем не менее можно сделать некоторые заключения. Прежде всего, следует заметить, что проектная интенсивность пучков на перечисленных выше ускорителях была получена не сразу после их пуска, а только через несколько лет напряженной работы. Сейчас на циклотроне SIN потери пучка составляют 0,3 μA при выведенном пучке 1 мА и сосредоточены, в основном, в районе вывода.

Линейный ускоритель обладает как преимуществами:

— автоматический вывод пучка;

— в импульсном режиме мгновенная интенсивность превышает 0,1 А,

так и недостатками:

— очень высокая рабочая частота и, как следствие, стоимость ВЧ-генератора;

— протяженный резонатор, для возбуждения которого требуется 40 + 50 МВт ВЧ-мощности в режиме нулевой интенсивности пучка, поэтому эффективность передачи ВЧ-мощности пучку оказывается приемлемой при интенсивности выше 0,3 А.

Основной недостаток циклотрона устраняется, если выбрать предложенный ранее циклотрон с разделенными орбитами [9], в котором сохраняется основное достоинство линейного ускорителя — эффективный вывод пучка. Тогда это предложение было несколько преждевременным, т.к. магнитная система в традиционном теплом варианте была неподходящей.

Сверхпроводимость, освоенная на ускорителях высоких энергий, может с успехом применяться в рассматриваемом диапазоне энергий. Если замена теплой катушки на сверхпроводящую в традиционном магните циклотрона [10] только снижает расходы на электропитание магнита, оставляя его размеры почти неизменными, то переход к малоапертурным СП-магнитам, в частности, синхротронным, дает целый ряд преимуществ:

— сокращает до минимума расходы энергии на возбуждение магнита;

— во много раз сокращает размеры и вес магнита;

— при разделении функций поворота пучка и фокусировки, частоты бетатронных колебаний частиц не зависят от их энергии, что снимает органичение на предельную энергию в циклотроне.

Сейчас в ФРГ завершается сооружение циклотрона с разделенными орбитами и сверхпроводящей магнитной системой [11] на энергию 38 МэВ. Запуск этого ускорителя позволит ответить на многие вопросы относительно машин этого типа.

Экстраполяция параметров циклотрона [11] на энергию 1 ГэВ [12] показывает перспективность этого типа машин для электроядерного реактора. Привлекательным выглядит предложение изначально разделить ускоряемый пучок на 10 каналов с отдельной сверхпроводящей магнитной системой синхротронного типа в каждом [13]. Высокий прирост энергии за оборот позволяет каждый магнитный канал выполнить в виде плоской спирали, а небольшая высота СП-магнитов — разместить все 10 каналов один над другим в общих гелиевых криостатах. Размещенные между ними общие для всех каналов теплые ВЧ-резонаторы сравнительно низкой частоты при интенсивности пучка 0,1 А обеспечивают коэффициент передачи ВЧ-энергии пучка 0,9.

Создание ускорителя с пучком протонов 1 ГэВ и током 0,1 А — задача сложная, но разрешимая при современном состоянии ускорительной техники. Какой вариант

ускорителя будет принят в ядерной энергетике, покажет будущее, но начинать эту работу нужно уже сейчас.

Заключение

На различных этапах развития ядерной энергетики ускоренные пучки заряженных частиц рассматривались как возможное альтернативное решение возникающих проблем. В конце 40-х годов стояла задача срочной организации производства делящихся материалов в достаточном объеме. В 70-е годы представлялось, что ресурсы разделительных установок исчерпываются, а в реакторах на быстрых нейтронах время удвоения топлива слишком велико. Тем не менее они были менее дорогостоящими и продолжали развиваться.

Сейчас, когда вопросы безопасности ядерной энергетики являются определяющими, пучки заряженных частиц представляются единственным средством полного исключения НЦР в реакторах и предотвращения неконтролируемого распространения ядерного оружия. Решение этих насущных задач в первую очередь определится тем, как быстро и экономично ускорители из прибора для физических экспериментов трансформируются в надежную и мощную промышленную установку. ОИЯИ и ЦЕРН объединяют ученых востока и запада Европы, и, думается, что объединение их усилий обеспечит решение этой задачи.

Литература

1. Васильков В.Г., Гольданский В.И., Джелепов В.П., Дмитриевский В.П. — АЭ, 1970, т.29, вып.3, с.152.
2. Carminati F., Klapisch R., Revol J.P., Roche Ch., Rubio J.A., Rubbia C. — «An Energy Amplifier for Cleaner and Inexhaustible Nuclear Energy Production Driven by a Particle Beam Accelerator». CERN/AT/93-47 (ET), 1993.
3. Давиденко В.А. — АЭ, 1970, т.29, вып.3, с.158.
4. Толстов К.Д. — Краткие сообщения ОИЯИ, 1993, 5[62]-93, с.5.
5. Jameson R.A. — In: «LAMPF Proton Linac Performance». Труды четвертого Всесоюзного совещания по ускорителям заряженных частиц. М.: Наука, 1975, т.1, с.131.
6. Craddock M.K. — «Recent Development of the Triumph Meson Factory». Труды пятого Всесоюзного совещания по ускорителям заряженных частиц. М.: Наука, 1977, т.1, с.145.
7. Willax H.A., the SIN Staff. — «Status of the Ring Cyclotron Project of the Swiss Institute for Nuclear Research (SIN)». Труды четвертого Всесоюзного совещания по ускорителям заряженных частиц. М.: Наука, 1975, т.1, с.224.
8. Андреев А.Г. и др. — Труды десятого Всесоюзного совещания по ускорителям заряженных частиц. Дубна, 1987, т.1, с.175.
9. Russel F.M. — Nucl. Instr. & Meth., 1963, v.23, p.229.
10. Blosser H.G. — «Characteristics of 400 Q^2/A MeV Superconducting Cyclotron». Труды пятого Всесоюзного совещания по ускорителям заряженных частиц. М.: Наука, 1975, т.1, с.212.

11. Trinks U. — «Tritron Status». Report on XXIX European Cyclotron Progress Meeting, Dubna, June 20-23, 1994. To be published.
12. Trinks U. — «Exotic Cyclotrons — Future Cyclotron». Lecture Given at CERN Accelerator School at LaHupe. To be published, 1994.
13. Шелаев И.А. — Краткие сообщения ОИЯИ, 1993, 5[62]-93, с.16.

Рукопись поступила 1 ноября 1996 года.

XJ9700067

УДК 539.142

ACCOUNTING OF NUCLEON CORRELATIONS FOR STUDY OF MOMENTUM DISTRIBUTIONS IN NUCLEI*

M.K.Gaidarov[1], *A.N.Antonov*[1], *S.E.Massen*[2], *G.S.Anagnostatos*[3]

Nuclon momentum distributions of the ^{12}C, ^{16}O, ^{40}Ca, ^{56}Fe, ^{208}Pb and some light neutron-rich nuclei are calculated by a model using the natural orbital representation and the experimental data for the momentum distribution of the ^{4}He nucleus. The model allows realistic momentum distributions to be obtained using only hole-state natural orbitals or mean-field single-particle wave functions as a good approximation to them. To demonstrate the model, different sets of wave functions were employed and the predictions were compared with the available empirical data and other theoretical results.

Учет нуклонных корреляций для изучения импульсных распределеиий в ядрах

М.К.Гайдаров и др.

Импульсные распределения нуклонов в ядрах ^{12}C, ^{16}O, ^{40}Ca, ^{56}Fe, ^{208}Pb и в некоторых легких нейтронно-избыточных ядрах рассчитаны с помощью модели, которая использует представление естественных орбиталей и экспериментальные данные об импульсном распределении ядра ^{4}He. Модель позволяет получить реалистические импульсные распределения, используя только естественные орбитали дырочных состояний либо одночастичные волновые функции среднего поля как хорошее приближение. Чтобы продемонстрировать возможности модели, использовались разные наборы волновых функций и были проведены сравнения с имеющимися экспериментальными данными и другими теоретическими результатами.

1. Introduction

The systematic investigations of the nucleon momentum distributions in nuclei extend the scope of the nuclear ground-state theory. The experimental situation in recent years makes it possible to study quantities such as: the nucleon momentum distribution $n(k)$ which is specifically related to the processes like the $(p, 2p)$, $(e, e'p)$ and (e, e') reactions, the

*The work is partly supported by the Bulgarian National Science Foundation under the Contracts Ф-406 and Ф527

[1]Institute of Nuclear Research and Nuclear Energy, Bulgarian Academy of Sciences, Sofia 1784, Bulgaria
[2]Department of Theoretical Physics, Aristotle University of Thessaloniki, Thessaloniki 54006, Greece
[3]Institute of Nuclear Physics, NCSR «Demokritos», Aghia Paraskevi-Attiki, 15310, Greece

nuclear photoeffect, meson absorption by nuclei, inclusive proton production in proton-nucleus collisions, and even some phenomena at low energies such as giant multipole resonances.

The main characteristic feature of the nucleon momentum distribution obtained by various correlation methods [1—7] is the existence of high-momentum components, for momenta $k > 2$ fm^{-1}, due to the presence of short-range and tensor nucleon correlations. We emphasize also the fact that theoretical results of the methods mentioned above as well as experimental data for $n(k)$ obtained by the y-scaling analysis of inclusive (e, e') experiments [8,9] confirm the conclusion that the high-momentum behaviour of the nucleon momentum distribution ($n(k)/A$ at $k > 2$ fm^{-1}) is almost the same for nuclei with mass number $A = 2$, 3, 4, 12, 16, 40, 56 and for nuclear matter (see [2], p.139). More generally, the above property of $n(k)$ is true for all nuclei with $A \geq 4$, and ^{4}He is the lightest nuclear system that exhibits the correlation effects via the high-momentum components of the nucleon momentum distribution. Since the magnitude of the high-momentum tail is proportional to the number of particles, this effect is associated with the nuclear interior rather than with the nuclear surface. This allows us to suggest a practical method to calculate the nucleon momentum distribution for nuclei heavier than ^{4}He (e.g., ^{12}C, ^{16}O, ^{40}Ca, ^{56}Fe, and ^{208}Pb) from that one of ^{4}He which is already known from the experimental data. In general, the knowledge of the momentum distribution for any nucleus is important for calculations of cross sections of various kinds of nuclear reactions.

In the last years the light exotic nuclei with $N/Z > 1$ are studing very intensively. The peculiarities of these nuclei start from $N/Z \approx 2$ when a deviation from the shell-model scheme of the nuclear levels is discovered (for instance, in ^{11}Be nucleus). In nuclei with $N/Z \approx 3$ (^{8}He, ^{11}Li) the neutron «halo» and associated anomalously large rms radius are observed. In the region $N/Z \approx 2.5$ (nucleus ^{10}Li) the nuclear structure is established as a core of $(A-1)$-particles in the ground state plus loosely-bound extra neutron. These peculiarities of the nuclei which have not been identified before show that the nuclear physics began investigating regions of nuclei with new feature. This induces our calculations on exotic nuclei momentum distribution based on the method suggested recently [10].

2. The Model

The model uses the transparency of the single-particle picture existing within the framework of the given correlation method by means of the natural orbital representation [11], where the proton momentum distribution normalized to unity has the form:

$$n(k) = \frac{1}{4\pi Z} \sum_{nlj} (2j+1)\, \lambda_{nlj} \left| \tilde{R}_{nlj}(k) \right|^2. \qquad (1)$$

In (1) $\tilde{R}_{nlj}(k)$ is the radial part of the natural orbital in the momentum space, λ_{nlj} is the natural occupation number for the state with quantum numbers (n, l, j) and

$$\sum_{nlj} (2j+1)\,\lambda_{nlj} = Z. \tag{2}$$

In the case of neutron momentum distribution Z has to be replaced by the number of the neutrons N. It was shown by the Jastrow correlation method (JCM) [6] that the high-momentum components of the total $n(k)$ caused by short-range correlations are almost completely determined by the contributions of the particle-state natural orbitals. This fact, together with the approximate equality of the high-momentum tails of $n(k)$ for all nuclei with $A \geq 4$, allows us to make the main assumption of this work, namely, that the particle-state contributions to the momentum distributions are almost equal for all nuclei with $A \geq 4$. Using the equality, we obtain the following general relation of the correlated proton momentum distribution of a nucleus (A, Z) with that one of the ^{4}He nucleus:

$$n^{A,Z}(k) = N\left[n^{^4\mathrm{He}}(k) + \frac{1}{4\pi}\left(\frac{1}{Z} \sum_{nlj}^{F_{A,Z}} (2j+1)\,\lambda_{nlj}^{A,Z}\,|\tilde{R}_{nlj}^{A,Z}(k)|^2 - \lambda_{1s_{1/2}}\,|\tilde{R}_{1s_{1/2}}^{^4\mathrm{He}}(k)|^2 \right)\right], \tag{3}$$

where

$$N = \left[1 + \frac{1}{Z} \sum_{nlj}^{F_{A,Z}} (2j+1)\,\lambda_{nlj}^{A,Z} - \lambda_{1s_{1/2}}^{^4\mathrm{He}} \right]^{-1}, \tag{4}$$

and $F_{A,Z}$ is the Fermi level for the nucleus (A, Z).

As shown in the previous papers the hole-state orbitals are almost unaffected by the short-range correlations and, therefore, the functions $\tilde{R}_{nlj}(k)$ can be replaced by the shell-model single-particle wave functions. The hole-state occupation numbers λ_{nlj} are close to unity within the JCM and we can set them equal to unity with good approximation. Thus the correlated nucleon momentum distribution can be calculated for any nucleus by means of the occupied shell-model wave functions and the momentum distribution of the ^{4}He nucleus which is taken from the experimental data [8] and which contains short-range correlation effects.

3. Calculations and Discussion

In this work we calculate the proton momentum distribution for nuclei ^{12}C, ^{16}O, ^{40}Ca, ^{56}Fe, ^{208}Pb and the nucleon momentum distributions for the Li,Be, B, and C isotopes. Empirical estimations for $n(k)$ are available for nuclei ^{12}C and ^{56}Fe [8].

In our calculations of proton momentum distributions we use two types of MFA single-particle wave functions: 1) single-particle wave functions obtained within the Hartree–Fock method by using Skyrme effective forces and 2) multiharmonic oscillator single-particle

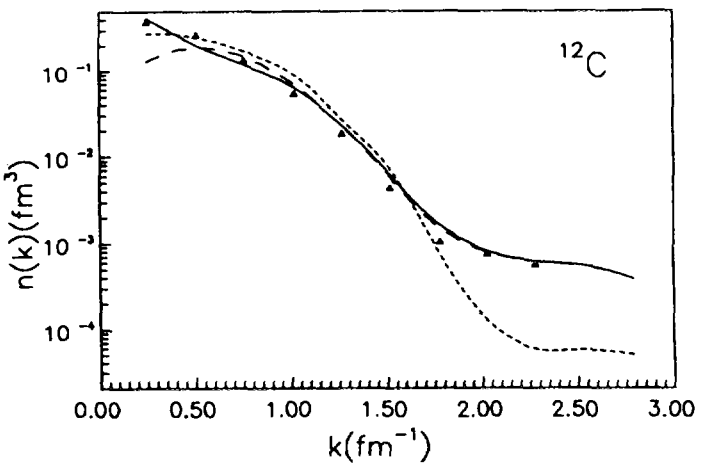

Fig.1. Proton momentum distribution $n(k)$ versus k of ^{12}C. Calculations by using single-particle wave functions from the multiharmonic oscillator shell model [13] are presented by solid line; and those by using the Hartree–Fock single-particle wave functions, by long-dashed line. The short-dashed line is $n(k)$ calculated in the Jastrow correlation method [6]. The solid triangles represent the data from [8]. The normalization is: $\int n(k)\, d^3 = 1$.

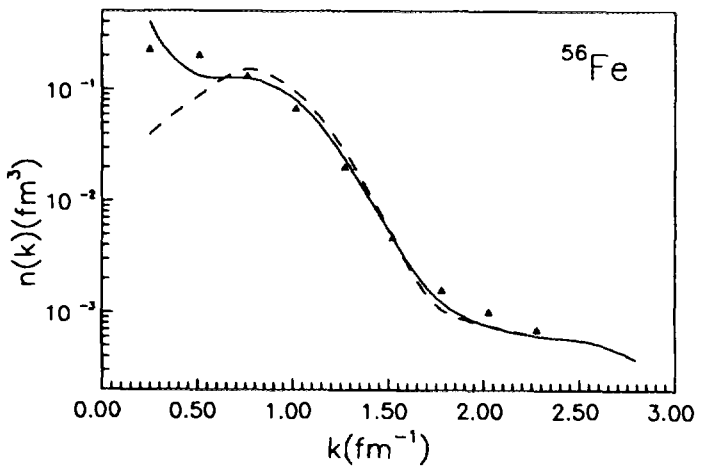

Fig.2. Proton momentum distribution $n(k)$ versus k of ^{56}Fe. Calculations by using single-particle wave functions from the multiharmonic oscillator shell model [13] are presented by solid line; and those by using the Hartree–Fock single-particle wave functions, by long-dashed line. The solid triangles represent the empirical data from [8]. The normalization is as in Fig.1.

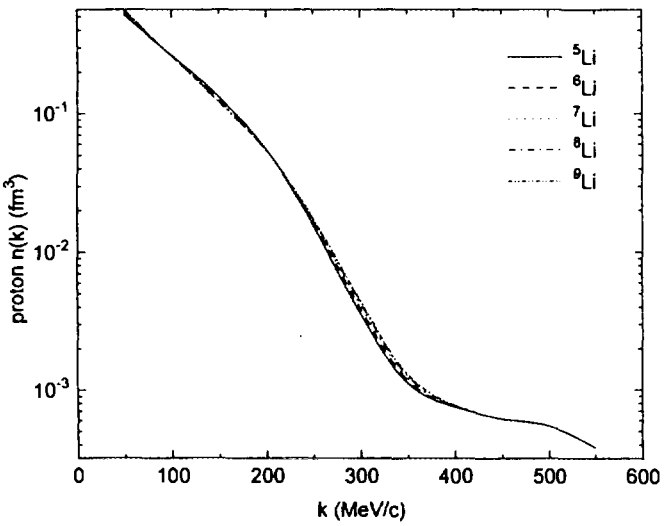

Fig.3. Proton momentum distribution in Li isotopes obtained by using harmonic-oscillator s.p. wave functions with $\hbar\omega$ defined by Eq.(5). The normalization is as in Fig.1

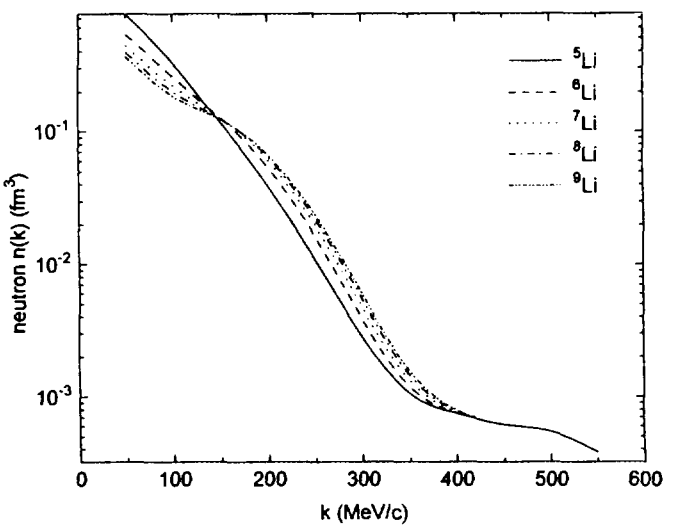

Fig.4. Neutron momentum distribution in Li isotopes obtained by using harmonic-oscillator s.p. wave functions with $\hbar\omega$ defined by Eq.(5). The normalization is as in Fig.1.

wave functions (with different values of the oscillator parameter for each state) which lead to a simultaneous description of ground-state radii and binding energies [12,13]. In addition to [13], in our calculations the multiharmonic oscillator s.p. wave functions are orthonormalized. In order to calculate the nucleon momentum distributions of the exotic nuclei we use harmonic-oscillator single-particle wave functions with an oscillator parameter which is A as well as N and Z dependent. This parameter gives, in principle, an estimate of the lowest energy level spacing and its variation with the number of the neutrons and protons. It represents also the average trend in the variation of the shape of the self-consistent nucleon-nucleus potential as a function of N and Z. In [14] an expression for $\hbar\omega$ as a function of N and Z is determined based on a formula for the nucleon charge radius which was proposed in [15] reproducing well the experimentally available RMS charge radii and the isotopic shifts of some even-even nuclei. It has the form:

$$\hbar\omega = 38.6A^{-1/3}[1 + 1.646A^{-1} - 0.191(N-Z)A^{-1}]^{-2}. \quad (5)$$

One can see from Figs.1 and 2 that the use of the single-particle wave functions from the multiharmonic oscillator shell model leads to better description of the experimental data for the central part of the momentum distribution than the use of the Hartree–Fock single-particle wave functions. In both cases the main deviations from the experimental data are for small momenta ($k \leq 0.5$ fm^{-1}). They are larger in the case when the Hartree–Fock s.p. wave functions are used and this is a common feature of the results for all nuclei considered. This is due to the well-known fact [16] that the Hartree–Fock method cannot give a realistic wave function for the 1s state in the ^{4}He nucleus. Namely this function ($\tilde{R}^{^4\mathrm{He}}_{1s_{1/2}}(k)$) takes part in the expression for $n(k)$ (Eq.(7)) in all nuclei. Both types of s.p. wave functions, however, give similar results for the middle part as well as for the tail of the momentum distribution in all cases considered. Concerning the exotic nuclei one can see from Fig.3 that all Li isotopes have almost the same proton momentum distributions. The small difference comes from the different values of $\hbar\omega = \hbar\omega(A, Z, N)$. The neutron momentum distributions of the same isotopes are presented in Fig 4.

The comparison of the results obtained by using different mean-field single-particle wave functions can be useful for the proper choice of the latter in the applications of the model to practical calculations of $n(k)$ in cases when the knowledge of this quantity is necessary.

4. Summary

Suggesting a practical method for realistic calculations of the nucleon momentum distribution in light, medium and heavy nuclei, we would like to test whether the high-momentum tail of the momentum distribution for any nucleus can be approximated by that

for ^{4}He. We also check to what extent this approximation affects the central part of the momentum distribution. The numerical results in this work confirm to a great extent the abilities of the suggested correlation model to give realistic estimations for the proton momentum distribution in ^{12}C and ^{56}Fe and to predict the behaviour of $n(k)$ in ^{16}O, ^{40}Ca, and ^{208}Pb nuclei. They are in agreement with the results for the proton momentum distribution in ^{16}O and ^{40}Ca obtained within other theoretical methods in which the correlation effects are incorporated using nuclear matter results and with some empirical data for ^{12}C and ^{56}Fe obtained using the y-scaling method. We also make predictions for the proton and neutron momentum distributions of exotic nuclei. The knowledge of the realistic momentum distributions obtained in this work would allow us to describe in a similar way as it is done in [17] the quantities which are directly measurable in processes of particle scattering by nuclei.

References

1. Antonov A.N., Hodgson P.E., Petkov I.Zh. — Nucleon Momentum and Density Distributions, Clarendon Press, Oxford, 1988.
2. Antonov A.N., Hodgson P.E., Petkov I.Zh. —Nucleon Correlations in Nuclei, Springer-Verlag, Berlin-Heidelberg-New York, 1993.
3. Benhar O., Ciofi degli Atti C., Liuti S., Salmé G. — Phys. Lett., 1986, v.177B, p.135.
4. Bohigas O., Stringari S.— Phys. Lett., 1980, v.95B, p.9.
5. Schiavilla R., Pandharipande V.R., Wiringa R.B. — Nucl. Phys., 1986, v.A449, p.219; 1990, v.64, p.364; Phys. Rev., 1992, v.C46, p.1741.
6. Stoitsov M.V., Antonov A.N., Dimitrova S.S. —Phys. Rev., 1983, v.C47, p.2455; Phys. Rev., 1993, v.C48, p.74; In Proc of the 6th Workshop on Perspectives in Nuclear Physics at Intermediate Energies (ICTP, Trieste, May 1993), World Scientific Publ., Singapore, p.236 (1994).
7. Antonov A.N., Kadrev D.N., Hodgson P.E. — Phys. Rev., 1994, v.C50, p.164.
8. Ciofi degli Atti C., Pace E., Salmé G. — Phys. Rev., 1991, v.C43, p.1155.
9. Day D.B., McCarthy J.S., Meziani Z.E., Minehart R., Sealock R., Thornton S.T., Jourdan J., Sick I., Filippone B.W., McKeown R.D., Milner R.G., Potterveld D.H., Szalata Z. —Phys. Rev. Lett., 1987, v.59, p.427.
10. Gaidarov M.K., Antonov A.N., Anagnostatos G.S., Massen S.E., Stoitsov M.V., Hodgson P.E. — Phys. Rev., 1995, v.C52, p.3026.
11. Löwdin P.-O. — Phys. Rev., 1955, v.97, p.1474.
12. Anagnostatos G.S. — Int. J. Theor. Phys., 1985, v.24, p.579.
13. Anagnostatos G.S. — Can. J. Phys., 1992, v.70, p.361.
14. Lalazissis G.A., Panos C.P. — Phys. Rev., 1995, v.C51, p.1247.

15. Nerlo-Pomorska B., Pomorski K. — Nucl. Phys., 1993, v.A562, p.180.
16. Ring P., Schuck P. — The Nuclear Many-Body Problem, Springer-Verlag, New York –Heidelberg–Berlin, 1980.
17. Gaidarov M.K., Antonov A.N., Dimitrova S.S., Stoitsov M.V. — Int. J. Mod. Phys. E, 1995, v.4, p.801.

Received on November 28, 1996.

XJ9700068

УДК 539.172.128.13
539.172.28.12
539.142.2

OVERLAP FUNCTIONS IN NUCLEAR CORRELATION METHODS AND DIRECT NUCLEON REMOVAL PROCESSES

S.S.Dimitrova[1,2], *M.K.Gaidarov*[1,3], *A.N.Antonov*[1,2,3], *M.V.Stoitsov*[1], *P.E.Hodgson*[2], *V.K.Lukyanov*[3], *E.V.Zemlyanaya*[3], *G.Z.Krumova*[4]

A theoretical method to obtain overlap functions and spectroscopic factors from a model one-body density matrix (OBDM) accounting for short-range nucleon-nucleon correlations is applied to describe one-nucleon removal processes on the ^{16}O and ^{40}Ca nuclei. The method allows the differential cross sections of (p, d) reactions and the momentum distributions of a transitions to a single-particle states from (e, $e'p$) reactions to be calculated. It is shown that the overlap functions obtained within the Jastrow correlation method lead to a satisfactory description of the quantities considered.

Функции перекрытия в ядерных корреляционных методах и прямые процессы с перемещением одного нуклона

С.С.Димитрова и др.

Теоретический метод получения функций перекрытия и спектроскопических факторов из модельной одночастичной матрицы плотности, учитывающий короткодействующие нуклон-нуклонные корреляции, используется для описания процессов с выбиванием одного нуклона из ядер ^{16}O и ^{40}Ca. Вычислены соответствующие дифференциальные сечения (p, d)-реакций, а также импульсные распределения переходов к одночастичным состояниям из (e, $e'p$)-реакций. Сравнение с экспериментом показало, что полученные функции перекрытия с учетом короткодействующих корреляций Ястрова позволяют удовлетворительно описать рассматриваемые величины.

1. Introduction

The one-nucleon removal reactions provide useful information about the nuclear structure and the mechanisms of the interaction processes. Such reactions have been used to extract spectroscopic factors from the observed reaction cross sections. The (p, d) reaction has been a reliable spectroscopic tool (see, e.g., [1–7]). Knock-out reactions initiated with electrons have been also used for studying single-particle properties of nuclei (e.g., [8–12]).

[1]Institute of Nuclear Research and Nuclear Energy, Bulgarian Academy of Sciences, Sofia 1784, Bulgaria.
[2]Nuclear Physics Laboratory, Department of Physics, University of Oxford, Oxford OX1-3RH, U.K.
[3]Joint Institute for Nuclear Research, Dubna 141980, Russia.
[4]Department of Physics, University of Rousse, Rousse 7017, Bulgaria.

In particular, the extracted data for the nucleon momentum distributions from the $(e, e'p)$ experiments for a variety of nuclei by means of the y-scaling method [13] show unambiguously the existence of high-momentum components in them.

In the one-nucleon removal reactions the measured momentum distribution for a transition to a discrete state α in the residual nucleus $\rho_\alpha(p_m)$ is expressed by the bound-state wave function which is the Fourier transform of the overlap wave function $\phi_\alpha(\mathbf{r})$ between the ground state wave function of the target $\Psi^{(A)}$ and the wave function of the final state of the residual nuclues $\Psi^{(A-1)}$ [14,15]. In the coordinate space $\phi_\alpha(\mathbf{r})$ is defined as

$$\phi_\alpha(\mathbf{r}) = \langle \Psi_\alpha^{(A-1)} \,|\, a(\mathbf{r}) \,|\, \Psi^{(A)} \rangle, \tag{1}$$

where $a^\dagger(\mathbf{r})$ and $a(\mathbf{r})$ are creation and annihilation operators for a nucleon with spatial coordinate $\mathbf{r}$ (spin and isospin coordinates are not put in evidence). In the mean-filed approximation (MFA) $\Psi^{(A)}$ and $\Psi^{(A-1)}$ are Slater determinants and the overlap wave function is identified with the single-particle wave function corresponding to the mean-field potential. In approaches going beyond the limits of the MFA (correlation methods) the overlap function is different from the MFA single-particle wave function. Therefore, the growing interest in the interpretation of the recent (p, d) and $(e, e'p)$ experimental data is motivated by the possibility to clarify the limitation of the nuclear mean-field picture and to find the extent to which the hole orbitals in nuclei are depleted by means of the experimentally based information. The overlap functions (1) are not orthonormalized. Their norm defines the spectroscopic factor of the level α

$$S_\alpha = \langle \phi_\alpha \,|\, \phi_\alpha \rangle \tag{2}$$

and the normalized overlap function is:

$$\tilde{\phi}_\alpha(\mathbf{r}) = S_\alpha^{-1/2} \phi_\alpha(\mathbf{r}). \tag{3}$$

The general relationship which connects the asymptotic behaviour of the one-body density matrix with the overlap functions of the $(A-1)$-particle system eigenstates [16] is of significant importance because it enables one to obtain quantities connected with them by means of the exact OBDM (or by a realistic one obtained with a given correlation method) of the ground state of the A-particle system. The one-body density matrix associated with the ground state $\Psi^{(A)}$ of the target nucleus with A nucleons is defined as

$$\rho(\mathbf{r}, \mathbf{r}') = \langle \Psi^{(A)} \,|\, a^\dagger(\mathbf{r})\, a(\mathbf{r}') \,|\, \Psi^{(A)} \rangle. \tag{4}$$

After inserting the complete set of eigenstates $\Psi_\alpha^{(A-1)}$ of the residual $(A-1)$-nucleus, Eq.(4) becomes:

$$\rho(\mathbf{r}, \mathbf{r}') = \sum_\alpha \phi_\alpha^*(\mathbf{r})\, \phi_\alpha(\mathbf{r}') = \sum_\alpha S_\alpha \tilde{\phi}_\alpha^*(\mathbf{r})\, \tilde{\phi}_\alpha(\mathbf{r}'), \tag{5}$$

where ϕ_α and $\tilde{\phi}_\alpha$ are the overlap functions (1) and (3), respectively, S_α is the spectroscopic factor (2) and the summation implicitly includes also the continuum states associated with all scattering channels of the $(A-1)$ system.

The aim of the present work is to test the applicability of the overlap functions, obtained from the asymptotic restoration procedure [17] (which uses a correlated OBDM from the Jastrow correlation method [18,19]) as realistic form factors within the DWBA analyses of pick-up reactions on ^{16}O and ^{40}Ca nuclei. We emphasize that our calculations give *absolute cross sections* with no normalizing factors. In addition, the theoretical results for the single-particle momentum distributions are compared with the available experimental ones from $(e, e'p)$ reactions on the same nuclei.

The results for the differential cross sections of (p, d)-pick-up reactions calculated within the DWBA with overlap functions as trial form factors are presented in Sec.2. In Sec.3 a comparison of the theoretical estimations for the single-particle nucleon momentum distributions with available experimental data for $(e, e'p)$-knock-out reactions is made. The concluding remarks are given in Sec.4.

2. Overlap Functions as Realistic Form Factors in the (p, d)-Pick-Up Reactions

It has been shown in [19] that the nucleon-nucleon correlations affect mainly the one-body characteristics of the particle states above the Fermi level, while the hole states are almost unaffected. Moreover, this fact was confirmed in [17] using the possibility to restore the overlap functions, the separation energies and the spectroscopic factors for bound $(A-1)$-particle eigenstates by means of the ground-state one-body density matrix of the target A-particle system. The overlap-, mean-field- and natural orbital wave functions are quite similar for the hole states in nuclei. This justifies the use of shell-model orbitals instead of overlap functions within DWBA calculations for such kind of nuclear states. This approximation, however, is no longer valid for the particle states where the overlap functions significantly differ from the mean-field wave functions. Therefore, neither natural orbitals nor shell-model wave function can be used instead of the particle-state overlap functions within the DWBA analysis of the experimental data for one-nucleon transfer reactions.

It has been shown in [16] that the radial part of the overlap function for the lowest bound state can be obtained by the radial part of the OBDM $\rho_{lj}(r, r')$ at $r' \equiv a \to \infty$:

$$\phi_{n_0 lj}(r) = \frac{\rho_{lj}(r, a)}{C_{n_0 lj} \exp(-k_{n_0 lj} a)/a}, \tag{6}$$

where

$$k_{nlj} = \hbar^{-1} \sqrt{2m(E_{nlj}^{(A-1)} - E_0^{(A)})} \tag{7}$$

depends on the separation energy $E_\alpha = E_{nlj}^{(A-1)} - E_0^{(A)}$. The separation energy is:

$$\varepsilon_{n_0lj} = \hbar^2 k^2_{n_0lj} / 2m \tag{8}$$

and the spectroscopic factor is:

$$S_{n_0lj} = \langle \phi_{n_0lj} | \phi_{n_0lj} \rangle. \tag{9}$$

The coefficient C_{n_0lj} can be obtained from the asymptotic form of the diagonal part of the radial OBDM. In principle, the overlap functions for all bound states of the $(A - 1)$ nucleon system can be constructed from the OBDM repeating the above procedure.

In order to test the role of the overlap functions as realistic form factors we have calculated using the DWUCK4 code [20] the (p, d) reaction on ^{16}O and ^{40}Ca at different incident proton energy. The overlap functions for the one-neutron removal from $1p$ and $1d$ states in ^{16}O obtained in [17] are compared in Fig.1 with the form factors calculated under two different approximations, namely the separation energy prescription (SEP) and the effective binding energy prescription (EBEP).

The differential cross section for the (p, d)-pick-up transitions is calculated within the DWBA approach using a zero-range interaction. It can be written in the form [20]:

$$\frac{d\sigma^{lsj}_{pd}(\theta)}{d\Omega} = \frac{3}{2} \frac{S_{lsj}}{2j+1} \frac{D_0^2}{10^4} \sigma^{lsj}_{DW}(\theta), \tag{10}$$

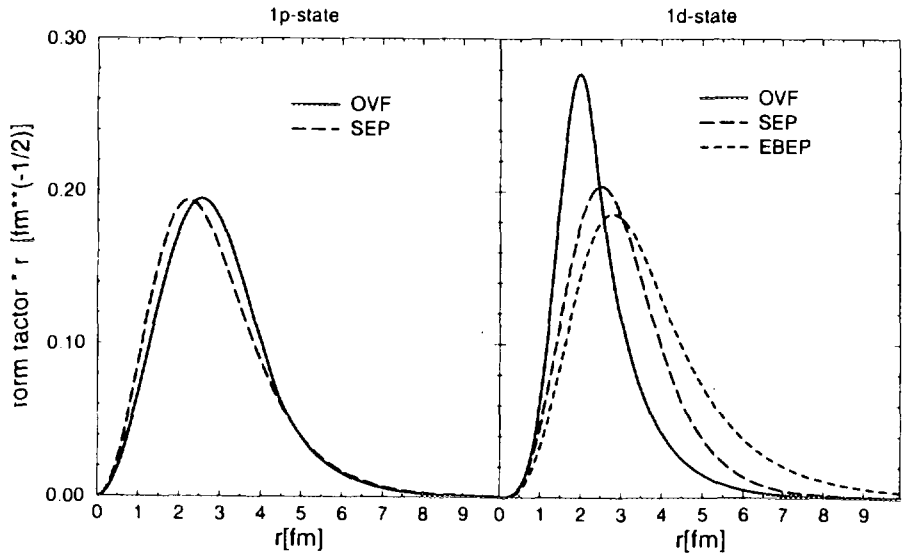

Fig.1. One-neutron removal overlap functions [17] (solid line) and form factors obtained within the SEP (long-dashed line) and EBEP (short-dashed line) for the transitions to the $1/2^-$ ground state and to the $5/2^+$ excited state in ^{15}O. All functions are normalized to unity

where S_{lsj} is the spectroscopic amplitude, j is the total angular momentum of the final state, $D_0^2 \approx 1.5 \times 10^4$ MeV·fm^3 and $\sigma_{DW}^{lsj}(\theta)$ is the cross section calculated by the DWUCK4.

The standard DWUCK4 procedure is performed by calculating the bound-neutron wave function using the SEP and EBEP and different sets of proton and deuteron optical model parameters are used. For our purposes the standard DWBA form factor was exchanged by that obtained in the framework of the one-body density matrix calculations and the spectroscopic factor S_{lsj} in (10) was taken to be equal to unity, since our overlap functions «contain» the sepctroscopic factor. Their normalization is (2):

$$4\pi \int |\phi_{lsj}(r)|^2 r^2 dr = S_{lsj}. \qquad (11)$$

As an example, the results for the differential cross sections of ^{16}O (p, d) reaction at E_p = 45.34 MeV calculated with overlap functions as trial form factors and with standard one are given in Fig.2. They are compared with the experimental data from [2,21]. As can be seen the shape of the angular distribution for the raction is well reproduced in both types of calculations. The use of overlap functions for the hole state leads to a good agreement with the data in their absolute values. This means that the residual interactions are taken into account sufficiently well as compared with the other models. Moreover, the spectroscopic factors deduced from the restoration procedure which are «contained» in the overlap functions are sufficient to reproduce the amplitude of the first maximum of the differential cross section for the hole states. The results for the transitions to the excited states are less

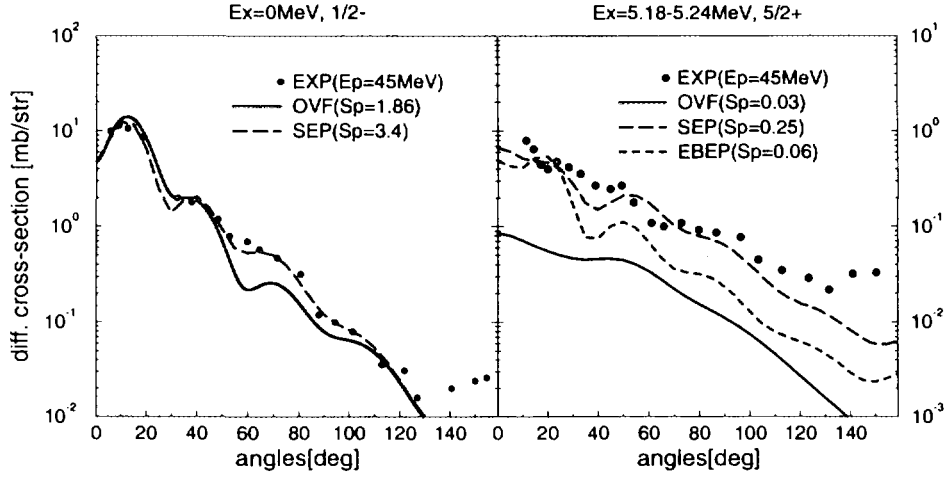

Fig.2. Differential cross section (solid line) for the ^{16}O (p, d) reaction at E_p = 45.34 MeV incident energy to the $1/2^-$ and $5/2^+$ states in ^{15}O. The DWBA results within the SEP (long-dashed line) and EBEP (short-dashed line) are shown. The experimental data [2,21] are given by the solid circles

Table. Spectroscopic factors for the ground states and the $5/2^+$ and $7/2^-$ excited states in ^{15}O and ^{39}Ca, respectively

^{15}O			^{39}Ca		
	$1/2^-$ (g.s.)	$5/2^+$		$3/2^+$ (g.s.)	$7/2^-$
OVF [17]	1.86	0.03	OVF [17]	3.60	0.08
SEP (E_p = 45 MeV)	3.40	0.25	SEP (E_p = 27.5 MeV)	2.30	0.32
EBEP (E_p = 45 MeV)		0.06	EBEP (E_p = 27.5 MeV)		0.16
			SEP (E_p = 65 MeV)	3.70	0.18
			EBEP (E_p = 65 MeV)		0.08

satisfactory. The reason is that the population of the particle states in ^{16}O and ^{40}Ca cannot be realistically described by the simple central pair-correlation included in the Jastrow-type OBDM.

In the Table we give the values of the spectroscopic factors of the transitions to the ground state and some excited states in ^{16}O and ^{40}Ca considered in our work. A comparison is made between the spectroscopic factors extracted from the OBDM [17] and those from the experimental data applying DWBA. Let us consider the spectroscopic factors of the transitions to the ground state, especially in ^{16}O. The problem of obtaining reasonable values for the spectroscopic factors in ^{16}O is well known and intensively studied [21,22]. The DWBA calculations with optical model parameters obtained from the elastic scattering analysis fail to reproduce the shape of the differential cross section [22]. By adopting the adiabatical deuteron optical model the shape of the cross section is well reproduced but the value of the spectroscopic factor exceeds the maximum allowed value of 2. However, using the overlap function from [17] which has a physically acceptable magnitude, one can achieve good agreement with the experimental cross section. We note that the results of the standard DWBA calculations depend significantly on the optical potentials used and on the incident energy. Let us look at the spectroscopic factors of the transitions to the excited states. It is seen that they vary among themselves more than the values for the ground states. They depend on the optical model parameters and the incident energies but also on the procedure applied to calculate the form factors. The spectroscopic factors of the overlap functions [17] do not always reproduce the magnitude of the experimental cross section. Obviously it is difficult to obtain reliable information about the absolute spectroscopic factors of the excited states unless a more refined OBDM is used.

We would like to emphasize that our calculations are absolute in contrast to the standard DWBA results which are adjusted to give the correct magnitude of the differential cross section. Especially for the particle states different prescriptions for calculating the form factor, which have acceptable justification, lead to quite different values for the spectroscopic factors. Thus it is worthwhile to investigate the differential cross sections of pick-up

reactions using absolute form factors which are extracted, however, from more sophisticated one-body density matrices, as for example the ones obtained by variational Monte Carlo calculations [23].

3. Momentum Distribution of a Transition to a Single-Particle State from (*e*, *e'p*) Reactions

The most direct way to get information on the single-particle wave functions is to study the one-nucleon knock-out reactions. In this Section we present some results of the calculations of the single-particle momentum distributions corresponding to a transition to a given s.p. state in comparison with the empirical data from the (*e*, *e'p*) reactions. In the Plane-Wave Impulse Approximation (PWIA) the energy ω and the momentum $\mathbf{q}$ lost by the electron are transferred to a proton with binding (missing) energy E_m and missing momentum $\mathbf{p}_m$. From the energy and momentum conservation laws the latter are determined by

$$E_m = \omega - E_p - T_{A-1}, \qquad \mathbf{p}_m = \mathbf{k}_p - \mathbf{q}, \tag{12}$$

where $\mathbf{k}_p$ and E_p are the momentum and the energy of the knocked-out proton, respectively, and T_{A-1} is the kinetic energy of the residual nucleus. The (*e*, *e'p*) cross section in the PWIA can be written in the form:

$$\frac{d^6\sigma}{de'd\mathbf{k}_p} = K\sigma_{ep}S(\mathbf{p}_m, E_m), \tag{13}$$

where K is a kinematical factor and σ_{ep} is the elementary electron-proton cross section [24]. The spectral function $S(\mathbf{p}_m, E_m)$ is the joint probability of finding a proton with separation energy E_m and momentum $\mathbf{p}_m$ inside the nucleus. For the transition to a discrete state α one can write

$$S(\mathbf{p}_m, E_m) = \rho_\alpha(\mathbf{p}_m)\,\delta(E_m - E_\alpha), \tag{14}$$

where the s.p. momentum distribution

$$\rho_\alpha(\mathbf{p}_m) = |\phi_\alpha(\mathbf{p}_m)|^2 \tag{15}$$

is the Fourier fransform squared of the overlap (1) between the initial and final nuclear state. The integration of the empirical data over the interval that covers the peak of the transition under study gives the single-particle momentum distribution $\rho_\alpha(\mathbf{p}_m)$. The spectroscopic factor S_α for a given α-state is determined by scaling the theoretical predictions for $\rho_\alpha(\mathbf{p}_m)$ to the experimental data.

In the present work we consider the s.p. momentum distributions in the ^{16}O and ^{40}Ca nuclei. As an example, we given in Fig.3 the momentum distribution for the transition to the second $1/2^+$ excited state in ^{39}K from the ^{40}Ca(*e*, *e'p*) reaction. In Fig.3 the

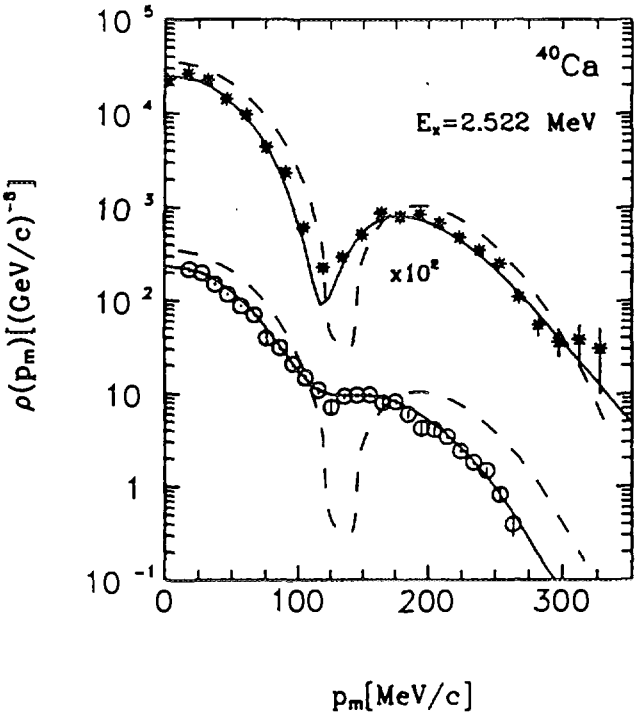

Fig.3. Momentum distribution for the transition to the second $1/2^+$ excited state in ^{39}K from ^{40}Ca (e, $e'p$) reaction. The calculations by using $2s$-overlap functions from [17] are presented by the dashed line. The stars and circles represent the empirical data measured in different kinematics [9]. The CDWIA calculations [9] are shown by solid lines

experimental data are given together with their Coulomb Distorted Wave Impulse Approximation (CDWIA) analysis [9] which is used to obtain spectroscopic factors for discrete transitions and rms radii for the various orbitals. The CDWIA calculations are performed employing different wave functions so that their rms radii are fitted to dscribe the data. In our method the necessity to use such parameters is avoided and we would like to emphasize the possibility of obtaining the momentum distribuitons in a consistent way on the basis of the OBDM corresponding to a correlated system. At the same time it is important to note the fact that the overlap functions from [17] are for neutron bound states. In the case of proton bound states some modifications due to the Coulomb asymptotic behaviour of the overlap functions have to be taken into account. Nevertheless, one can see that the calculated results for the momentum distributions are close to the experimental data. Especially this can be seen from Fig.3 where the minimum in the momentum distribution for the transition leading to the $1/2^+$ state in the ^{39}K at 2.522 MeV is well described. Our calculations show that generally the shape of the momentum distributions of the transitions can be adequately described by mean-field wave functions for momenta up to the Fermi momentum k_F ($\approx$ 250 MeV/c). Measurements over a more extended range of the momenta and with better accuracy are necessary to test the various bound-state wave functions.

4. Conclusions

In the present work a new method for theoretical studies of the one-nucleon removal processes is suggested. It is shown that the overlap functions of the $(A-1)$-particle system eigenstates obtained in [17] by using the general relationship [16] which connects the

asymptotic behaviour of the OBDM with them can be successfully applied as realistic form factors to calculate the differential cross sections of ^{16}O (p, d)- and ^{40}Ca (p, d)-pick-up reactions at various incident energies. The results of our calculations demonstrate that the obtained angular distributions do not need remormalization by introducing the spectroscopic factors. The overlap functions provide a physical and model-independent definition of the spectroscopic factors. The angular distributions are in good agreement with the experimental data in their absolute values for the ground states and less satisfactory for the excited states.

Our calculations of the s.p. momentum distributions of various orbitals in ^{16}O and ^{40}Ca describe satisfactorily the empirical data obtained by the (e, $e'p$)-knock-out reactions at momenta below the Fermi momentum. The results are also in agreement with the CDWIA calculations using bound-state wave functions evaluated in a mean-field potential. New measurements should be done at higher momenta where the SRC effects on the momentum distribution are sizable. Using the correct asymptotic behaviour of the proton overlap function in the procedure [17] and more realistic OBDM, one can expect that the resulting overlap functions will be able to describe more accurately the experimental single-particle momentum distributions.

Acknowledgements

This work was partly supported by the Agreement for Scientific Cooperation between the Bulgarian Academy of Sciences and the Royal Society, the Protocol for joint research work between INRNE (Sofia) and JINR (Dubna) and by the Bulgarian National Science Foundation under the Contracts Nos.Φ-406 and Φ-527. Two of us (S.S.D. and A.N.A.) would like to thank the Royal Society for financial support during their visits to the University of Oxford and the Laboratory of Nuclear Physics for the kind hospitality. A.N.A. and M.K.G. are grateful to the Laboratory of Theoretical Physics at JINR for support during their visits to Dubna.

References

1. Glashausser C., Kondo M., Rickey M.E., Rost E. — Phys. Lett., 1965, v.14, p.113.
2. Preedom B.M., Snelgrove J.L., Kashy E. — Phys. Rev., 1970, v.C1, p.1132.
3. Ross P.G. et al. — Nucl. Phys., 1975, v.A255, p.187.
4. Källne J., Fagerström B. — Phys. Scr., 1975, v.11, p.79.
5. Hosono K. et al. — Nucl. Phys., 1980, v.A343, p.234.
6. Abegg R. et al. — Phys. Rev., 1989, v.C39, p.65.
7. Matoba M. et al. — Phys. Rev., 1993, v.C48, p.95.
8. Frullani S., Mougey J. — Adv. Nucl. Phys., 1984, v.14, p.1.
9. Kramer J. — Ph. D. thesis, Amsterdam (1990) (unpublished).
10. Lapikas L. — Nucl. Phys., 1993, v.A553, p.297c.
11. Van der Steenhover G. et al. — Nucl. Phys., 1988, v.A480, p.547.
12. Den Herder J.W.A. et al. — Nucl. Phys., 1988, v.A490, p.507.
13. Ciofi degli Atti C., Pace E., Salme G. — Phys. Rev., 1991, v.C43, p.1155.

14. Berggren T. — Nucl. Phys., 1965, v.72, p.337.
15. Bang J.M., Gareev F.A., Pinkston W.T., Vaagen J.S. — Phys. Rep., 1985, v.125, p.253.
16. Van Neck D., Waroquier M., Heyde K. — Phys. Lett., 1993, v.B314, p.255.
17. Stoitsov M.V., Dimitrova S.S., Antonov A.N. — Phys. Rev., 1996, v.C53, p.1254.
18. Stoitsov M.V., Antonov A.N., Dimitrova S.S. — Phys. Rev., 1993, v.C47, p.R455.
19. Stoitsov M.V., Antonov A.N., Dimitrova S.S. — Phys. Rev., 1993, v.C48, p.74.
20. Langanke K., Maruhn J.A., Koonin S.E. — Computational Nucl. Phys. 2: Nucl. Reactions, Springer-Verlag, Berlin–Heidelberg–New York, 1993, p.88.
21. Snelgrove J.L., Kashy E. — Phys. Rev., 1969, v.187, p.1246.
22. McAllen G.M., Pinkston W.T., Satchler G.R. — Particle and Nuclei, 1970–71, v.1, p.412.
23. Pieper S.C., Wiringa R.B., Pandharipande V.R. — Phys. Rev., 1992, v.C46, p.1742.
24. De Forest T. Jr. — Nucl. Phys., 1983, v.A392, p.232.

Received on October 17, 1996.

XJ9700069

УДК 575:24: 595.773.4

MOLECULAR ALTERATIONS UNDERLYING THE SPONTANEOUS AND γ-RAY-INDUCED POINT MUTATIONS AT THE WHITE LOCUS OF DROSOPHILA MELANOGASTER

M.V.Alexandrova, I.L.Lapidus, I.D.Alexandrov, A.L.Karpovsky

The *white* locus in *D.melanogaster* was selected as a target gene for the study of the mutational spectra of spontaneously arising and radiation-induced gene mutations in a whole organism. Analysis of 6 spontaneous and 73 γ-ray-induced *white* mutations by a combination of cytological, genetic and molecular techniques revealed that on the chromosomal and genetic levels all spontaneous mutations showed themselves to be point mutants. The share of such mutants among all heritable radiation-induced gene mutations is about 40%, whereas the rest ones are due to exchange breaks (8%) as well as multilocus, single-locus or partial-locus (intragenic) deletions (52%).The DNAs from 4 spontaneous and 17 γ-ray-induced point mutants were analysed by *Southern* blot-hybridization. The three spontaneous and 7 radiation mutants showed an altered DNA sequence at the left (distal) half of the *white* gene due to insertion or DNA rearrangement. The rest (58%) of the radiation-induced point mutations did not indicate any alternations in this part of the gene as detected by this technique and probes employed.

The investigation has been performed at the Department of Radiation Safety and Radiation Researches, JINR.

Молекулярные изменения, обусловливающие спонтанные и индуцированные γ-излучением точковые мутации в локусе white у Drosophila melanogaster

М.В.Александрова, И.Л.Лапидус, И.Д.Александров, А.Л.Карповский

Локус *white* у *D.melanogaster* был избран в качестве гена-мишени для изучения спектра спонтанных и радиационно-индуцированных генных мутаций в целостном организме. Комплексный цито-генетико-молекулярный анализ 6 спонтанных и 73 индуцированных γ-излучением мутаций *white* показал, что на хромосомном и генетическом уровнях все спонтанные мутации проявляют себя как точковые. Доля таких мутаций среди наследуемых радиационно-индуцированных составляет около 40%, тогда как остальные обусловлены хромосомным разрывом при формировании обменных аберраций (8%), либо мультилокусными, однолокусными или частичными (внутригенными) делециями (52%). ДНК от 4 спонтанных и 17 радиационных мутантов точковой природы была изучена с помощью блот-гибридизации по Саузерну. Установлено, что 3 спонтанных и 7 радиационных мутаций имеют молекулярные изменения в левой (дистальной) половине гена, обусловленные инсерациями и/или структурными перестройками ДНК. Остальные

из изученных точковые радиационно-индуцированные мутации (58%) не содержат изменений в этой части гена, выявляемых данным методом и пробами, использованными в работе.

Работа выполнена в Отделе радиационной безопасности и радиационных исследований ОИЯИ.

I. Introduction

Summing up the main fundamental generalizations of the classical radiation genetics in the fields concerning gene mutation processing, H.Muller in his Nobel lecture had particularly laid stress among the others that the radiation-induced point (on the chromosomal level) mutations in animal cells are similar to the natural (spontaneous) ones in all features on which the comparison had been done [1]. This generalization founded mainly on the data from the genetical and/or cytological experiments with *Drosophila* before molecular era in modern biology and genetics is basic so far to our risk estimation procedure using the doubling dose method [2].

The current studies of the molecular nature of the point mutations arising spontaneously at the different loci of *Drosophila* (*Hw*, *w*, *ry*, *f*, etc.) had unequivocally shown that the bulk of them had resulted from insertion of the dispersed, repetitive DNA sequences, such as mobile elements or transposons [3].

On the other hand, the first results of the molecular analysis of point mutations induced by sparsely ionizing radiation at some of these *Drosophila loci* (*w*, *ry*) indicated that the main part of such mutants have arisen through large changes in the gene, especially deletions [4,5]. Recent analysis of radiation-induced HPRT- and APRT-deficient mutants of mammalian cells indicates also deletions as the major type genetic lesion recovered [6,7].

Thus, as the first molecular data show, the genetic alterations underlying the spontaneous and radiation-induced gene/point mutations in *Drosophila* germ cells seem to be qualitatively different, but the number of tested mutants are small. Moreover, spontaneously arising and radiation-induced mutations have been isolated in the genotypicly different *Drosophila* strains the difference of which on fine molecuar structure of gene studied and/or on DNA repair may determine the peculiarities of spectra of the gene mutations recovered.

To study this issue more precisely, the complex (genetic, cytogenetic, molecular) analysis of spontaneous and γ-ray-induced gene mutations in the different loci (*white*-w, *vestigial*-vg) and genotypes (*wild-type D-32*, *c(3)G*, *phr-*) of *Drosophila melanogaster* was started. In this communication, we present the genetic and cytogenetic characteristics of spontaneous and γ-ray-induced (5-60 Gy) gene mutations at the *w* locus from wild-type D-32 line as well as the first data on the molecular nature of some point mutations among them analyzed by *Southern* blot-hybridization.

II. Materials and Methods

The spontaneous *w* mutations were recovered in the large-scale experiments (1987—1994 years) described earlier [8,9], and γ-ray-induced ones were obtained as has been described by Alexandrov [10]. All transmissible *w* mutations were analysed by conventional

cytology of the polytene chromosomes to discriminate the exchange (intra- or interchromosomal) mutations from point (not associated with cytologically detectable chromosomal changes) ones. To detect the whole or partial deletions of the *w* gene, a sensitive and reliable genetic test on visible complementation with w^{sp} was employed using the more sensitive w^{spA} allele described earlier [11]. Isolation of genomic (from mutant and wild-type flies) and plasmid DNA, digestion of these DNAs with various restriction enzymes, ^{32}P-labelling of the probes by nick-translation and Southern blot-hybridization were performed according to standard procedures [12].

III. Results

According to data of cytological and fine genetic (complementation) analysis (Table) all 6 of spontaneous *w* mutations found have the point intragenic lesions since they show a normal chromosomal *3C2* region where the *w* locus lies as well as complementing phenotype over w^{spA} (the mutation type of the complementers). The analogous analysis of 73 γ-ray-induced *w* mutations revealed more complex spectrum of the radiation-induced gene mutations consisting of at least five different mutation types (Table): (i) exchange mutations showing the chromosome rearrangements involving translocations or inversions, one of two breakpoints of which passes through the site of the gene under study; (ii) multilocus

Table. Spectra of spontaneous and γ-ray-induced white mutations in Drosophila sperms classified by fine genetic and cytological analysis

	γ-ray dose, Gy					
	0	5	10	20	40	60
Number of mutants isolated / Number of F_1 progeny studied	6/267466	5/69375	10/60954	15/37955	39/57897	4/5994
Mutation types:						
Exchange mutations	0	0	0	1(0.06)*	3(0.09)	2(0.5)
Multilocus deletions	0	2(0.4)	2(0.2)	4(0.27)	15(0.38)	1(0.25)
Point mutations:						
Total	6(1.0)	3(0.6)	8(0.8)	10(0.67)	21(0.53)	1(0.25)
Complementers**	6	1	5	5	17	1
Partial complementers	0	0	2	2	1	0
Non-complementers	0	2	1	3	3	0

*The number in parentheses indicates the fraction of the total for given dose.
**See text.

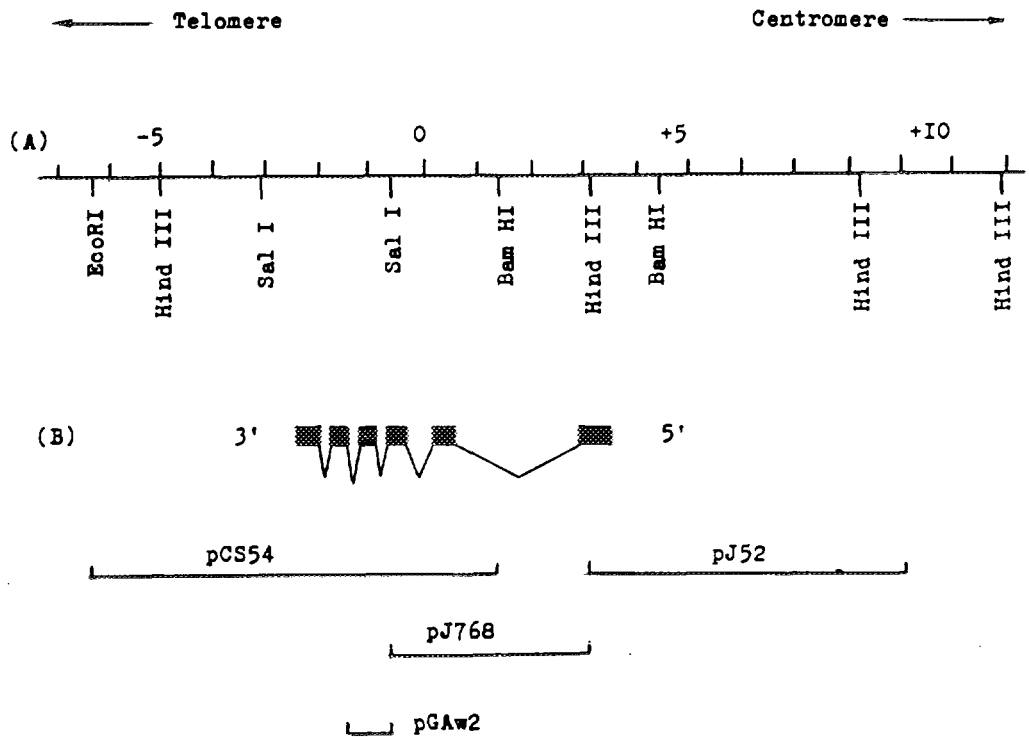

Fig.1. (A). Restriction map of the w^+ locus of D-32 wild-type strain in kilobases (1 kb = 1000 bp). The coordinate 0.0 is the point of the *copia* insertion in the allele w^a [13]. Restriction sites were determined by *Southern* blot-hybridization of digested genomic DNA with *pCS54*, *pJ768* or *pJ52* probes [14] which were a kind gift of Dr. V.Anashchenko (Gatchina). (B). The position of the w^+ trascript (six exons as the black boxes and five introns as the broken lines) as determined by [15]. *pCS54*, *pJ768*, *pJ52*, and *pGAw2* probes contain sequences from other *Drosophila* strains [5,14]

deletions being themselves the losses of the *w* locus and the adjacent genes; (iii) point mutations with the putative intragenic lesions much of which behave as complementers, and the rest of them do either (iv) the partial complementers or (v) the non-complementers. The complementation patterns of the last two mutation types indicate on the presumed partial or total losses of the *w* gene, respectively [5].

Thus, 100% of spontaneous and almost 40% (29/73) of γ-ray-induced *w* point mutations demonstrate the same phenotypic, cytological and genetic features as if supporting the generalization of the classical radiation genetics above noted. Does it mean that the molecular alterations underlying these point mutations are the same consisting of base-pair changes, insertions or very small intragenic deletions?

To answer this intriguing question, 4 spontaneous and 17 γ-ray-induced *w* point mutants were further analysed by blot-hybridization, permitting the detection of deletions

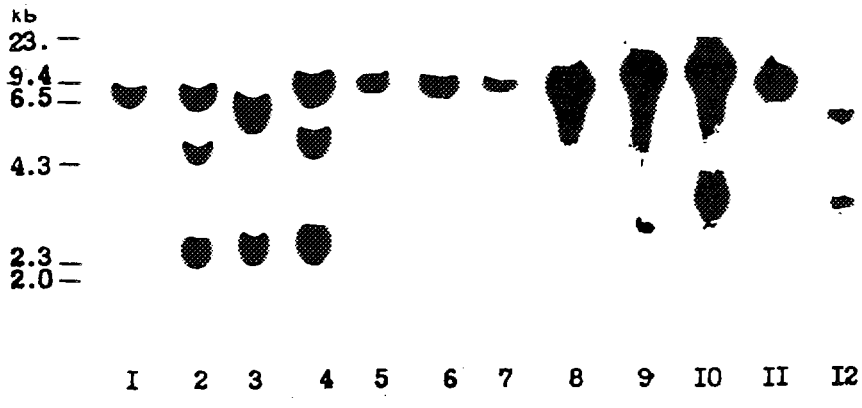

Fig.2. *Southern* blot-analysis of DNAs from spontaneous and γ-ray-induced *w* point mutations after digestion with *Hind III* and hybridization with *pCS54*; lines 1—12: wild-type D32 strain; spontaneous mutants *w88c45*, *w88d46*, *w92l1*; radiation mutants *w74b29*, *w83f29*, *w88d32*, *w81k2*, *w81k6*, *w87g67*, *w87g14*, *w78f39*, respectively.

or inversions with a minimal size of about 100 bp as well as the gain or loss of restriction enzyme sites. Taking into account the fact that eye pigmentation is about zero or uniformly reduced in mutants studied as in ones mapping usually at the distal end of the locus [5], DNAs from spontaneous and radiation-induced mutants and wild-type flies of the *D-32* strain were digested with *Hind III*, *Bam HI or Sal I* restriction enzymes and hybridizated with *pCS54*, *pJ768* or *pGAw2* probes which permit the detection of the genetic lesions located in this half of the w^+ gene (Fig.1).

As the hybridization pictures show, digestion of DNA from the spontaneous mutant *w88c45* with *Hind III* and following hybridization with *pCS54* give rise to three fragments of 8.2, 5.0 and 2.9 kb, instead of a single 8.2 kb in wild-type flies (Fig.2, lines 1 and 2). Hybridization of *w88c45* DNA with *pJ768* result in the same three fragments (data not shown) indicating that molecular alteration (insertion with duplication) affects the genic fragment between coordinates -0.7 and $+1.4$ kb which is in common for both probes (Fig.1). Spontaneous mutant *w92l1* is identical to *w88c45* (Fig.2,lane 4), whereas *w88d46* seems to be a deletion derivative of these mutants since it shows 2.9 kb being in common for three mutants studied and a new fragment of 5.9 kb instead of two fragments of 8.2 and 5.0 kb (Fig.2, line3). Therefore, these hybridization results indicate an interruption of the *w* sequence in the spontaneous mutants studied by a gain of genetic material the investigation of nature of which requires the further experiments.

DNAs from the γ-ray-induced mutants *w74b29* (40 Gy), *w81k2* (10 Gy), *w83f29* (40 Gy), *w87g14* (10 Gy) and *w88d32* (40 Gy) did not show any discrepancies from w^+ allele in hybridization pattern after digestion with *Hind III* and blotting with *pCS54* (Fig.2, lines 5,8,6,11,7). The analogous results were obtained for the radiation mutants *w67a* (40 Gy),

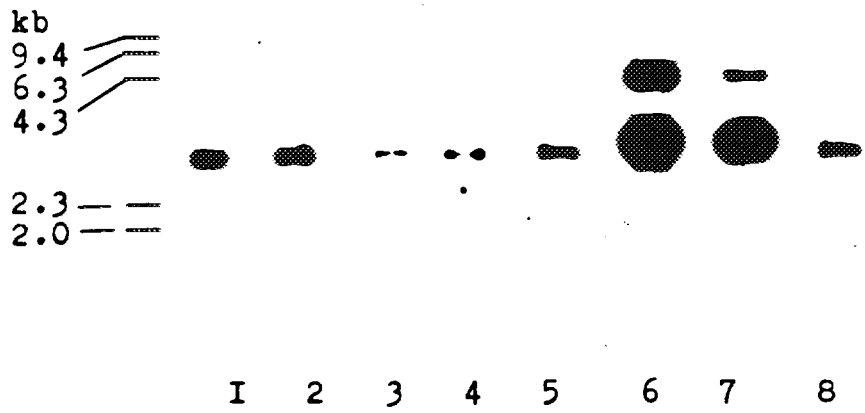

Fig.3. Southern blot-analysis of DNAs from spontaneous and γ-ray-induced point white mutations after digestion with *Sal I* and hybridization with *pGAw2*; lines 1—8: spontaneous mutants *w88c45*, *w88d46*, *w94l2*; wild-type D-32 strain; radiation mutants *w81k8*, *w81k6*, *w81k7*, *w87g75*

w71k (40 Gy), *w81k3* (10 Gy) and *w83c20* (40 Gy) (data not shown).The single Hind III fragment of 8.2 kb in wild-type flies is replaced by three new fragments of 8.5, 5.0, 2.7 kb; 14.0, 3.3, 2.7 kb and 6.5, 3.3, 2.7 kb in *w81k6* (10 Gy), *w87g67* (20 Gy) and *w87f39* (5 Gy), respectively (Fig.2, lines 9,10,12) and by two new fragments of 9.4, 4.7 kb and 8.5, 2.7 kb in *w72b* (40 Gy) and *w81k4* (10 Gy), respectively (data not shown). Therefore, all of these mutants display the gross structural alterations in the left half of the *w* gene being likely consequences of insertion or DNA rearrangement events.

To study this point more precisely, the digestion with *Sal I* and hybridization with *pGAw2* probe were performed for the three spontaneous and four γ-ray-induced mutants. As the results obtained show, the wild-type flies, spontaneous (*w88c45*, *w88d46*, *w94l2*) and two radiation-induced (*w81k8*, *w87g75*) mutants indicate a single *Sal I-Sal I* fragment of 2.7 kb (Fig.3, lines 1—5,8) discovered by *pGAw2* (Fig.1). This means that the genic fragment between coordinates − 3.05 and − 0.6 is not affected in these mutants. Therefore, these results support independently our notion claimed above that the genetic alterations in the spontaneous mutants are located within the genic fragment between coordinates − 0.6 and + 1.4 affecting the second and third exons and first and second introns of the *w* gene (Fig.1).

The single *Sal I-Sal I* fragment of 2.7 kb in wild-type flies is replaced in *w81k6* (10 Gy) and *w81k7* (20 Gy) by two new fragments of 4.3 and 3.0 kb (Fig.3, lines 6 and 7) showing that these γ-ray-induced mutants are structural ones, but the lesions detected earlier elsewhere in *Hid III -Hind III* fragment of 8.2 kb by hybridization with *pCS54* (Fig.2, line 9) are precisely located in *Sal I — Sal I* fragment in contrast with site of lesions in *Sall-Bam HI* fragment in the spontaneous mutants.

IV. Conclusion

The results presented in this communication indicate the presence of the large molecular changes in 3 spontaneous and 7 γ-ray-induced point *w* mutations displaying the similar phenotype, genetics and cytology. The rest 10 radiation mutants studied seem not to show any alterations at least after *Hind III*-digestion and hybridization with the large gene fragment (*pCS54*). It is quite possible that step-by-step analysis of the whole DNA sequence in these mutants with a set of a short fragments as probes will permit one to detect more small alterations than those revealed by a large probes used firstly. It is of interest and important the more so that the share of point mutants without detectable molecular changes (likely, a true point mutations with base-pair changes) in our set of γ-ray-induced *w* mutations (10/17 or almost 58%) is much higher than that obtained by others for the *white* [5] or *rosy* [4] loci in *Drosophila* germ cells after *X*-ray-irradiation. The further our ongoing experiments must ascertain the reason of this discrepancy and give a new information on the molecular spectra of the heritable gene mutations induced by densely ionizing radiation (neutrons, heavy ions).

Acknowledgements

This work is partly supported by grant from Russian State Program «Frontiers in Genetics» and grant 96-04-50741 from RFFR.

References

1. Muller H. — In: Herskowitz I., Genetics, Little, Brown and Co., Boston and Toronto, 1965, Suppl., p.562.
2. UNSCEAR, Genetic effects of Radiation, United Nations, Vienna, 1986.
3. Bingham P.M., Zachar Z. – In: Mobile DNA, Berg D.E., Howe M.M., Editors, Amer. Soc. Microb., Wash. D.C., 1989, p.485.
4. Cote B. et al. — Genetics, 1986, v.112, p.769.
5. Pastink A. et al. — Mutat. Res., 1987, v.177, p.101.
6. Grosovsky A.J. et al. — Genetics, 1986, v.113, p.405.
7. Philips E.N. et al. — Rad. Res., 1995, v.143, p.155.
8. Alexandrov I.D. — Drosophila Inform. Service, 1992, v.71, p.213.
9. Alexandrov I.D., Alexandrova M.V. — Doklady Acad. Sci. (Rus), 1994, v.337, No.4,p.550.
10. Alexandrov I.D. — Mutat. Res., 1984, v.127, p.123.
11. Alexandrov I.D. — Drosophila Inform. Service, 1982, v.58, p.7.

12. Sambrook J. et al. — Molecular cloning — Lab. Manual. CSHL Press, Cold Spring Harbor, NY, 1989.
13. Levis R. et al. — Proc.Natl. Acad. Sci. (USA), 1982, v.79, p.564.
14. Sang H.M. et al. — EMBO J., 1984, v.3, p.3079.
15. O'Hare K. et al. — J. Mol. Biol., 1984, v.180, p.437.

Received on November 12, 1996.

XJ9700070

УДК 539.173

МОГУТ ЛИ СУЩЕСТВОВАТЬ В ПРИРОДЕ СВЕРХТЯЖЕЛЫЕ ЭЛЕМЕНТЫ?

Ю.Ц.Оганесян

На основе экспериментальных и теоретических результатов последних лет по обнаружению острова стабильности тяжелых деформированных ядер вблизи оболочек $Z = 108$ и $Z = 162$ рассматриваются радиоактивные свойства более тяжелых нуклидов вблизи замкнутых сферических оболочек с $Z = 114$ и $Z = 184$. Из рассмотрения следует, что для ядер с $Z = 106 + 108$ и $N = 180 + 184$ можно ожидать большие времена жизни вплоть до $T_{1/2} \sim 10^8$ лет. Подобные сверхтяжелые и сверхстабильные нуклиды, образующиеся в процессе нуклеосинтеза, могли сохраниться в малых количествах до наших дней. В отличие от всех предыдущих экспериментов, нацеленных на поиск спонтанного деления ядра $^{298}114$ (EkaPb), предлагается постановка опытов по обнаружению редких событий радиоактивного распада ядер с $Z = 106 + 108$ (EkaW-EkaOs) с массой около 290. Предполагается, что распад этих нуклидов будет представлять радиоактивный ряд (четвертый к известным трем цепочкам естественной радиоактивности), состоящий из последовательных β- и α-распадов, который может окончиться спонтанным делением. Показано также, что в опытах по поиску коррелированных распадов сверхтяжелых природных излучателей может быть достигнута чувствительность обнаружения вплоть до 10^{-21} г/г в предположении, что время жизни радиоактивных ядер $\geq 10^8$ лет.

Работа выполнена в Лаборатории ядерных реакций им. Г.Н.Флерова ОИЯИ.

Can Superheavy Elements Exist in Nature?

Yu.Ts.Oganessian

Basing on the experimental and theoretical results obtained in recent years on the discovery of the stability domain of heavy deformed nuclei near the shells with $Z = 108$ and $N = 162$, the radioactive properties of heaviest nuclides near the closed spherical shells with $Z = 114$ and $N = 184$ are considered. From the examination of these properties it follows that one can expect long half-lives of up to $T_{1/2} \sim 10^8$ years for the nuclei with $Z = 106 + 108$ and $N = 180 + 184$. Such superheavy and superstable nuclides, formed in the nucleosynthesis process, can still exist in small quantities to the present day. In distinction to all previous experiments aimed at the search for the spontaneous fission of a $^{298}114$ (EkaPb) nucleus, it is proposed to perform experiments on the discovery of rare events of the radioactive decay of nuclei with $Z = 106 + 108$ (EkaW-EkaOs) and $A = 290$. It is assumed that the decay of these nuclides will represent the radioactive chain (the fourth one besides the three known chains of natural radioactivity), consisting of sequential β- and α-decays, which may end with spontaneous fission. It is also shown that in the experiments on the search for natural radioactivity correlated decays of superheavy nuclei the detection sensitivity of up to 10^{-21} g/g may be achieved, assuming that the half-life of radioactive nuclei is $\geq 10^8$ years.

The investigation has been performed at the Flerov Laboratory of Nuclear Reactions, JINR.

История вопроса

Экспериментальные и теоретические исследования потенциальной энергии ядер указывают на значительное влияние структуры на форму ядра в основном и деформированном состояниях.

Это обстоятельство играет решающую роль в стабильности очень тяжелых ядер, не устойчивых к спонтанному делению.

Действительно, еще в ранних работах В.Майерса, В.Святецкого [1,2], С.Нильссона [3], В.Струтинского [4], В.Пашкевича [5], Р.Никса [6] и др. было показано, что для сверхтяжелых ядер, в отсутствие макроскопического (капельного) барьера деления, учет эффекта ядерной структуры приводит к появлению барьера деления, резко уменьшающего вероятность спонтанного деления. При всей неопределенности расчетов проницаемости барьера деления запреты на спонтанное деление в области замкнутых сферических оболочек $Z = 114$ и $N = 184$ [7,8] оценивались величиной ~ 10^{30-35}.

Нельзя было исключить (хоть и с малой вероятностью), что эти запреты столь велики, что время жизни сверхтяжелых ядер относительно спонтанного деления будет $\geq 10^8$ лет (без эффекта ядерных оболочек ~ 10^{-20}с). Другие возможные типы распада — α- и β-распады — определяются, как известно, разностью масс и структурой ядер вблизи основного состояния, которые также зависят от силы эффекта ядерных оболочек. Различные формулы масс указывали на высокую стабильность сверхтяжелых ядер относительно и этих типов распада [9,10].

Тогда подобные сверхтяжелые и сверхстабильные ядра, если бы они образовались в процессе нуклеосинтеза, могли сохраниться в природе до наших дней. Предполагалось, что основным типом распада сверхтяжелого ядра будет спонтанное деление.

Идея поиска сверхтяжелых элементов по спонтанному делению принадлежит Г.Н.Флерову и его сотрудникам, которые в 1972—1988 гг. предприняли широкомасштабные эксперименты по обнаружению спонтанного деления в различных природных образцах и в космических лучах.

Исследовались различные минералы, обедненные ураном (основной и, фактически, единственный природный источник фона спонтанного деления с $T_{s.f.} = 10^{16}$ лет), концентраты продуктов химического обогащения тяжелых металлов платино-свинцовой группы, метеоритное вещество и многие другие образцы.

Не вдаваясь в детальный анализ всех экспериментов, которые читатель может найти в оригинальных работах [11—14] и обзорах [15,16], приведем конечный результат. Предполагалось, что деление будет испытывать тяжелое ядро с $Z \geq 110$. Ожидалось, что среднее число нейтронов, возникающих при делении столь тяжелого ядра, будет ~10. Ввиду высокой проникающей способности нейтронов можно было использовать массивные образцы весом 20 + 30 кг, для которых измерялись редкие события множественного рождения нейтронов.

Для исключения фона от взаимодействия космических мюонов с образцом аппаратура помещалась в подземную лабораторию на глубину ~ 1000 м водного эквивалента.

Путем тщательного анализа содержания урана в образцах удалось достигнуть высокой чувствительности, соответствующей регистрации одного события в месяц с $\nu \geq 3$. Отдельные события, зарегистрированные в длительных экспозициях, которые нельзя было отнести к распаду урана, имели, к сожалению, малую множественность ($\nu \sim 2$). Эти события разумно было интерпретировать как верхнюю границу ожидаемого эффекта. Она составляла ~ 10^{-14} г/г в предположении, что сверхтяжелое ядро имеет период полураспада $T_{1/2} \sim 10^8$ лет.

Естественно, отсутствие эффекта в подобных экспериментах может найти различные объяснения. Если сверхтяжелые ядра образовались в процессе нуклеосинтеза, то вполне вероятно, что их время жизни значительно меньше 10^8 лет. Однако в целом вопрос о существовании в природе ядер, значительно тяжелее урана, остается открытым.

Ниже мы попытаемся проанализировать эту проблему с современных позиций.

Искусственный синтез и свойства трансактинидных элементов

Известно, что все элементы с $Z > 100$ были синтезированы в ядерных реакциях под действием тяжелых ионов. Однако в любой комбинации мишень — ион реакция слияния ведет к образованию ядер со значительным дефицитом нейтронов; все продукты распада компаунд-ядра значительно удалены от линии β-стабильности. Наоборот, в нуклеосинтезе изотопы имеют значительный нейтронный избыток и расположены за линией β-стабильности.

Вместе с тем, эксперименты, предпринятые в Дармштадте [17—19] и в Дубне [20—23] по синтезу новых элементов в реакциях холодного слияния (на основе Pb-мишени) и горячего слияния (на основе мишени из тяжелых изотопов актиноидов), привели к открытию более 30 новых изотопов с $Z = 102 + 112$ и $N = 150 + 165$. Эти ядра расположены далеко от вершины предполагаемого острова стабильности $Z = 114$ и $N = 184$. Однако все изотопы с $Z \geq 106$ преимущественно испытывали α-распад, что свидетельствовало об их высокой стабильности относительно спонтанного деления.

Объяснение этого явления было найдено в более совершенных и детальных расчетах коллективного движения ядер.

З.Патиком, Р.Смолянчуком и А.Собичевским [24—26] было показано, что влияние ядерной структуры на процесс деления требует учета высоких порядков деформации для описания ядерных форм. С другой стороны, при проникновении через потенциальный барьер структурной природы массовый коэффициент (инерциальный фактор) испытывает значительные вариации в процессе деформации ядра. Учет этих факторов привел к нетривиальным предсказаниям существования подъема стабильности деформированных ядер вблизи оболочек с $Z = 108$ и $N = 162$.

Целенаправленные эксперименты, поставленные нами, по синтезу самых тяжелых изотопов элементов с $Z = 104$, 106, 108 и 110 показали резкий подъем стабильности ядер по мере приближения к $N = 162$ [21—23]. Поскольку четно-четные изотопы с $Z = 104$ испытывают спонтанное деление, а все синтезированные изотопы с $Z \geq 106$ — α-распад, было проведено прямое сравнение теории с экспериментом. При этом было получено хорошее количественное согласие.

Это важное обстоятельство, так как если теперь данный теоретический метод расчета применить к области более тяжелых ядер, то можно получить значительно более реалистические предсказания свойств сверхтяжелых нуклидов, чем это было сделано раньше.

Эта работа проводится авторами [22,23], и ряд уже полученных результатов заслуживает обсуждения в контексте рассматриваемой нами проблемы.

Ожидаемые свойства сверхтяжелых ядер

Как видно из рис.1, амплитуда оболочечной поправки при переходе от деформированной оболочки $Z = 108$, $N = 162$ к сферической $Z = 114$, $N = 184$ меняется в небольших пределах [25]. Однако с ростом числа нейтронов меняется макроскопическая (капельная) составляющая потенциальной энергии ядра, что приводит к значительным изменениям барьера деления ядер. Вследствие этого резко возрастает стабильность сверхтяжелых ядер относительно спонтанного деления.

Расчетные значения периодов α-распада — T_α приведены в нижней части рисунка. Видно, что, например, для ядер с $Z = 110$ переход от $N = 162$ к $N = 184$ приводит к увеличению парциального периода T_α в 10^{13} раз.

Однако величина T_α для изотопов более тяжелого ядра с $Z = 114$ и $N = 180 + 184$ составляет всего $\sim 10^3$ с. Конечно, такое ядро не может существовать в природе.

Вместе с тем, протонная и нейтронная оболочки имеют разную силу и тем самым дают разный вклад в полный эффект результирующей стабильности ядра. Если сильно изменить число протонов, то стабильность ядра будет определяться в основном эффектом нейтронной оболочки $N \sim 184$. Последние расчеты Р.Смолянчука позволяют это сделать [27].

На рис.2 представлены расчетные периоды T_α и $T_{s.f.}$ для изотопов 104 и 114 элементов в зависимости от числа нейтронов. Виден огромный эффект сферической оболочки $N = 184$. Парциальные периоды спонтанного деления и α-распада ядра $^{288}104$ составляют $3 \cdot 10^7$ и $3 \cdot 10^{17}$ лет, соответственно. Для ядра $^{298}114$ парциальный период спонтанного деления составляет также более 10^7 лет, в то время как $T_\alpha \approx 10^3$ с.

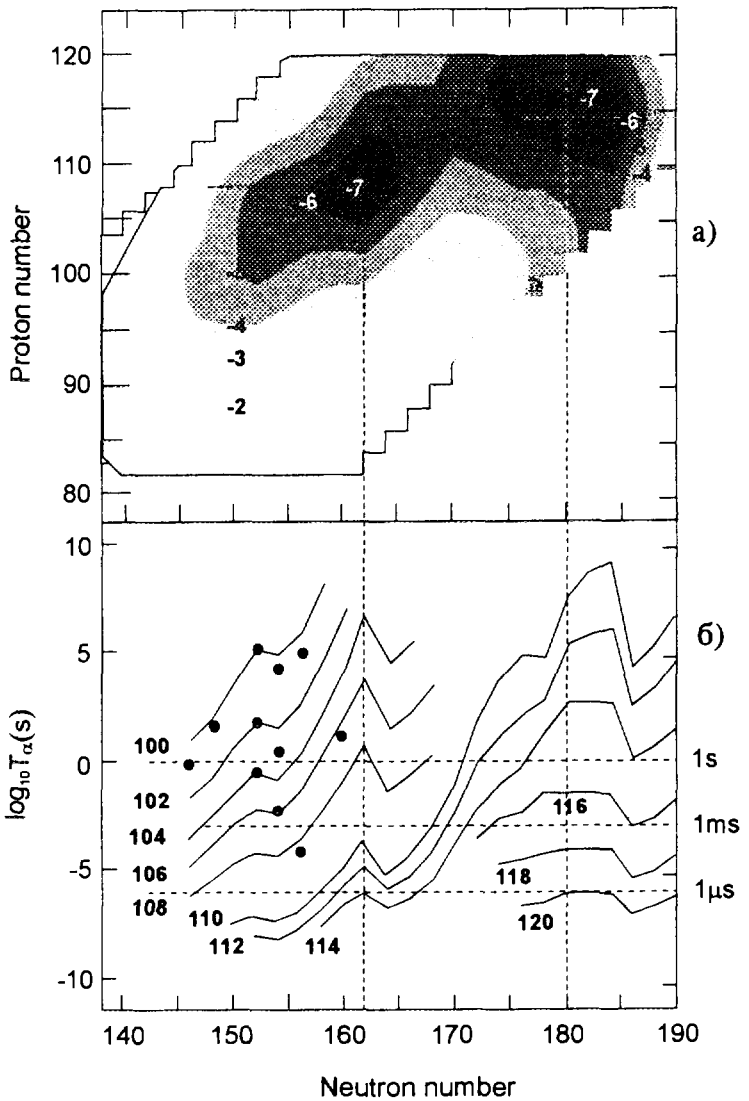

Рис.1. а) Контурная карта расчетных значений амплитуды оболочечных поправок (в МэВ) к макроскопической (капельной) энергии деформации ядер с различными Z и N. б) Парциальные периоды α-распада (в секундах) в зависимости от числа нейтронов для изотопов с $Z \geq 100$. Сплошные линии — расчет [25], точки — экспериментальные значения

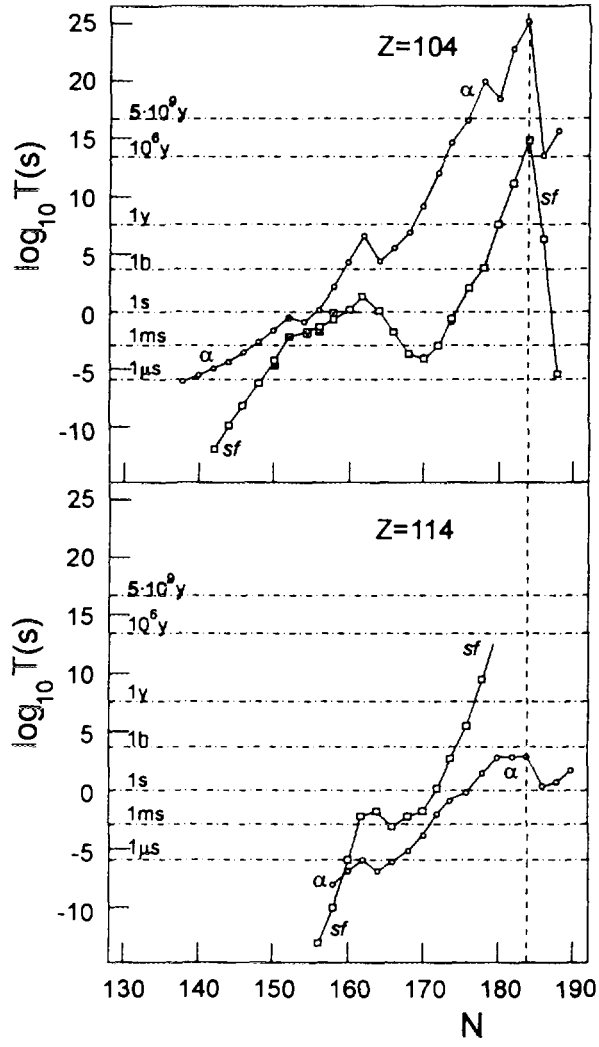

Рис.2. Парциальные периоды спонтанного деления (квадраты) и α-распада (кружки) изотопов 104 и 114 элементов. Открытые символы — расчет [26,27], черные точка и квадраты — экспериментальные значения, полученные для изотопов с $Z = 104$. Сплошные линии проведены через расчетные значения

В любом случае эти значения на много порядков величины выше тех значений $T_{s.f.}$ и T_{α}, которые предсказывались и подтверждены экспериментом для изотопов, расположенных вблизи деформированной нейтронной оболочки $N = 162$.

Могут ли существовать в природе сверхтяжелые элементы?

Приведенное выше, в качестве примера, ядро $^{288}104$ будет, по всей вероятности, испытывать β^--распад. Однако в процессе последовательных β^--распадов парциальные периоды T_{β^-} образующихся ядер с $Z > 104$ будут возрастать вследствие приближения к линии β-стабильности. Другая ситуация с α-распадом и спонтанным делением. При наличии эффекта нейтронной оболочки $N = 184$ увеличение Z должно усиливать эффект протонной оболочки по мере приближения к $Z = 108$. Это обстоятельство должно привести к увеличению стабильности более тяжелых ядер относительно спонтанного деления в пределах $N = 180 + 184$. Наоборот, с ростом Z парциальные периоды ядер относительно α-распада будут уменьшаться.

Если наложить условие, что полное время жизни ядра должно быть $\geq 10^8$лет, то круг возможных кандидатов сильно ограничивается областью Z от 106 до 108 и N от 180 до 184. Более детальные расчеты по макромикроскопической теории еще сильнее сузят эти границы, если не отвергнут целиком возможность существования столь стабильных нуклидов.

Однако, в любом случае, проблема поиска сверхтяжелых природных излучателей меняется коренным образом. Наиболее стабильным ядром будет не EkaPb, как предполагалось раньше, а нуклиды на 6 + 8 атомных номеров ниже (область EkaW—EkaOs) с массой $A \sim 290$. Подобные ядра будут испытывать последовательные β- и α-распады с образованием новых ядер, удаляющихся от оболочки $N = 184$. Для четно-четных ядер подобная цепочка последовательных распадов должна окончиться спонтанным делением. Длина цепочек будет определяться конкуренцией между α- и β^--излучением на всех ступенях распада. Для длинных цепочек не исключено, что конечно ядро, удаленное от оболочки $N = 184$, но все еще обладающее избытком нейтронов, будет испытывать ту моду деления, которая характеризуется узким симметричным распределением масс осколков, высокой кинетической энергией и малым числом нейтронов. Подобный тип деления был наблюден в области тяжелых актинидных ядер [28].

Постановка экспериментов по поиску сверхтяжелых элементов в природе

Постановка экспериментов по поиску сверхтяжелых элементов теперь будет сильно отличаться от ранее предпринятых опытов [11—16]. По сути задача сводится к поиску нового радиоактивного ряда, отличного от уже известных цепочек распада ^{235}U, ^{238}U и ^{232}Th. Основным признаком обнаружения этой цепочки будут последовательные α-распады и β-распады, которые могут закончиться спонтанным делением. В

качестве объектов исследования наиболее перспективными могут быть гомологи вольфрама, рения, осмия. Пока, не имея всех расчетных данных, предпочтение можно отдать EkaOs.

Измерительная аппаратура должна быть рассчитана на поиск редких событий α-распадов с эффективностью, близкой к 100%, с высоким энергетическим и пространственным разрешением. Если процессы химического обогащения Os и EkaOs одинаковы, то можно определить предельную чувствительность эксперимента по обнаружению радиоактивного распада EkaOs. Для исходного вещества Os весом 1 г (приготовленного в виде тонкого слоя ~ 0,1 мг/см^2) обнаружение одного акта коррелированного распада в год (α–α- или s.f.-корреляции) будет соответствовать концентрации ядер EkaOs в образце на уровне $5 \cdot 10^{-14}$ при $T_{1/2} = 10^8$ лет.

Это соответствует распространенности EkaOs в земной коре на уровне $5 \cdot 10^{-22}$ г/г.

Поскольку массы ядер стабильного Os и гипотетического EkaOs отличаются в 1,5 раза, можно существенно повысить обогащение EkaOs и, соответственно, понизить предел обнаружения сверхтяжелого ядра. Возможно также увеличить чувствительный объем детектора и вес образца.

Заключение

1. Экспериментальные исследования последних лет по синтезу тяжелых элементов и расчеты макромикроскопической модели ядер предсказывают значительное повышение стабильности сверхтяжелых сферических ядер вблизи оболочки $N = 184$.

2. Не исключено, что в области трансактинидных элементов изотопы с массой ~ 290 могут обладать сверхвысокой стабильностью, сопоставимой с природными радиоактивными ядрами ($T_{1/2} \geq 10^8$ лет). Более определенные заключения о радиоактивных свойствах наиболее долгоживущего ядра и цепочек его распада могут быть сделаны на основе расчетов масс и вероятностей деления сверхтяжелых ядер с учетом эффекта ядерных оболочек. Экспериментальная проверка теоретических данных может быть осуществлена в экспериментах по синтезу и исследованию радиоактивных свойств изотопов 112 и 114 элементов с $N = 170 \div 171$ и $174 \div 175$, образующихся в реакциях слияния ядер ^{238}U и ^{244}Pu с ионами ^{48}Ca.

3. Возможность образования таких сверхтяжелых ядер в процессе нуклеосинтеза требует отдельного рассмотрения. Необходимы расчеты парциальных периодов $T_{s.f.}$ и T_β актинидных ядер с $Z = 98 \div 102$ с $N = 184 \div 190$.

4. Эксперименты по поиску сверхтяжелых природных ядер, по всей вероятности, должны быть нацелены на обнаружение последовательных α- и β-распадов, а также спонтанного деления.

Современные методы регистрации радиоактивного распада и детальный анализ событий дают возможность, в принципе, обнаружить новые излучатели в природных образцах вплоть до уровня их содержания ~ 10^{-21} г/г в предположении, что их период полураспада составляет 10^8 лет.

Благодарности

Приношу благодарности моим коллегам д-рам И.Зваре, С.Дмитриеву, М.Иткису, Ю.Музычке и Б.Пустыльнику за ценные замечания при обсуждении данной работы.

Считаю своим приятным долгом поблагодарить д-ров Р.Смолянчука и А.Собичевского за интересные и плодотворные дискуссии о стабильности сверхтяжелых ядер.

Благодарю Е.Щукину за помощь в оформлении статьи.

Литература

1. Myers W.D., Swiatecki W.J. — Nucl. Phys., 1966, 81, p.1.
2. Myers W.D., Swiatecki W.J. — Ark. Phys., 1967, 36, p.343.
3. Nilsson S.G. et al. — Nucl. Phys., 1969, A131, p.1.
4. Brack M. et al. — Rev. Mod. Phys., 1972, 44, p.320.
5. Pashkevich V.V. — Nucl. Phys. A, 1971, 169, p.275.
6. Nix J.R. — Ann.Rev. Sci., 1972, 22, p.65.
7. Gareev F.A., Kalinkin B.N. — Phys. Lett., 1966, 22, p.500.
8. Meldner H. — Ark. Phys., 1967, 36, p.593.
9. Ю.А.Музычка, В.В.Пашкевич, В.М.Струтинский — ЯФ, 1968, 8, с.716.
10. Muzychka Yu.A.— Phys. Letters 28B, 1969, p.539.
11. Флеров Г.Н., Тер-Акопьян Г.М., Скобелев Н.К. — ЯФ, 1974, 20, с.472.
12. Флеров Г.Н. и др — ЯФ, 1977, 26, с.449.
13. Флеров Г.Н. и др. — Радиохимия, 1982, 24, с.782.
14. Dmitriev S.N. et al.— JINR Rapid Commun., N5(31)88, Dubna, 1988, p.13.
15. Flerov G.N., Ter-Akopian G.M. — Pure and Appl. Chem., 1981, 53, p.909.
16. Flerov G.N., Ter-Akopian G.M. — in Treatise on Heavy Ion Physics, Edit. D.A.Bromley, New York, Plenum Press, 1985, v.4, p.333.
17. Muenzenberg G. — Rep. Prog. Phys., 1988, 51, p.57.
18. Hofmann S. et al. — Z. Phys., 1995, A350, p.277.
19. Hofmann S. et al. — Z. Phys., 1996, A354, p.229.
20. Oganessian Yu.Ts. — Radiochim. Acta, 1984, 37, p.113.
21. Lazarev Yu.A. et al. — Phys. Rev. lett., 1994, 73, p.624.
22. Lazarev Yu.A. et al. — Phys. Rev. Lett., 1995, 75, p.1903.
23. Lazarev Yu.A. et al. — Phys. Rev., 1996, 54, p.620.
24. Patyk Z., Sobiczewski A. — Nucl. Phys., 1991, A533, p.132.

25. Smolanczuk R., Skalsi J., Sobiczewski A. — Phys. Rev., 1995, C52, p.1871.
26. Smolanczuk R., Sobiczewski A. — Low Energy Nuclear Dynamics (World Scientific, Singapore, 1995), p.313.
27. Smolanczuk R. — Third Intern. Conf. on Dynamical Aspects of Nucl. Fission, Casta-Papernicka, Slovac Rep. August 30 — Sept. 4, 1996. In press.
28. Hulet E.K. et al. — Phys. Rev. C, 1989, 40, p.770.

Рукопись поступила 14 ноября 1996 года.

XJ9700071

УДК 539.173

STUDY OF DEEP SUBBARRIER REACTIONS ON A Pb TARGET

B.I.Pustylnik, L.Calabretta*, M.G.Itkis, E.M.Kozulin, Yu.Ts.Oganessian, A.G.Popeko, R.N.Sagaidak, A.V.Yeremin, S.P.Tretyakova

The fission and evaporation cross section of a ^{224}Th compound nucleus has been measured in the reaction $^{16}O + ^{208}Pb$ up to 15 MeV below the fusion barrier, deeply in the subbarrier energy region, which made it possible to analyse cross sections by 8 orders of magnitude lower than the geometrical cross section of heavy ion interaction with nuclei.

The investigation has been performed at the Flerov Laboratory of Nuclear Reactions, JINR.

Изучение глубоконеупругих реакций на свинцовой мишени

Б.И.Пустыльник и др.

Сечения деления и испарительных реакций были измерены в реакции $^{16}O + ^{208}Pb$ в глубокоподбарьерной области энергий, вплоть до энергии 15 МэВ ниже барьера слияния ядер, что дало возможность для анализа сечений на 8 порядков величины меньше, чем геометрическое сечение взаимодействия ядер.

Работа выполнена в Лаборатории ядерных реакций им. Г.Н.Флерова ОИЯИ.

1. Introduction and Experiment

In the present work the fission and evaporation cross section of a ^{224}Th compound nucleus has been measured in the reaction $^{16}O + ^{208}Pb$ up to 15 MeV below the fusion barrier, deeply in the subbarrier energy region, which made it possible to analyse cross sections by 8 orders of magnitude lower than the geometrical cross section of heavy ion interaction with nuclei. The fission experiment has been carried out at the beam of the tandem accelerator (NFIN, Catania, Italy). Single fission fragments were detected in the backward angular range of 90-164° and 198-270° by using mica dielectric detectors with an area of 170 cm^2 [1]. Evaporation excitation functions have been measured for *xn*-, *pxn*-, and αxn-decay channels of the compound nuclei ^{224}Th produced at the beam of the U-400 cyclotron (FLNR, JINR, Dubna). Products of complete fusion reactions were separated from the bombarding ions and products of transfer and deep inelastic reactions with the aid of the kinematic separator VASSILISSA. Recoil nuclei and their α-decay were observed by means of a detector system installed in the separator focal plane. It consists of a pair of

* Laboratorio Nazionale del Sud, Catania, Italy

large-area time-of-flight detectors and a silicon detector array consisting of eight independent strips with the energy resolution of 30 keV for α-particles in the energy range of 5-9 MeV [2].

A great body of experimental data was recently obtained on subbarrier fusion cross sections, however, in all these investigations fusion-fission and fusion-evaporation cross sections are obtained within a wide high-energy range, while in the subbarrier region there are only several points, where the energy is below the barrier by 1-8 MeV. In addition, recently some works have been published, where the cross sections of evaporation reactions differ by one order of magnitude, see [3] and references therein. Our interest in the study of such deep subbarrier interaction is connected not only with a possibility of investigating the fusion cross section and discussing the mechanism of subbarrier reactions enhancement in the case of spherical nuclei interaction, but also with a possibility of investigating structural effects in different fission modes of compound nuclei, produced in reactions with heavy ions. Earlier this type of investigations has been carried out only in reactions with light charged particles [4].

2. Experimental Results and Discussion

The estimation of the fission and evaporation cross section necessarily involves both the details of the compound nucleus formation process and relative competition between fission and other modes in a ^{224}Th compound nucleus decay process.

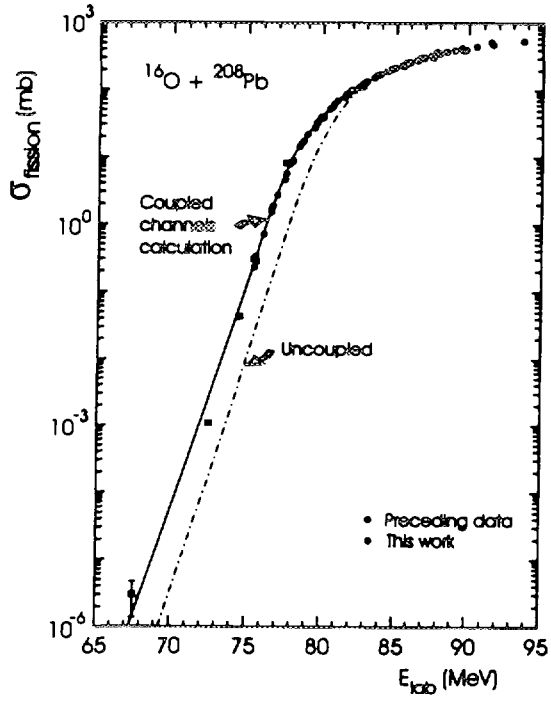

Fig.1

Calculations of the fusion cross sections were tested: (a) within the Wong approximation; (b) within the standard approximation of an inverted parabola with a nuclear potential in the form of Igo; (c) by the introduction of the vibrational zero-point motion of the surface; (d) by the method of coupled channels using a standard software package CCFUS. Figure 1 presents our experimental fission cross sections, data from different works joined in Ref.3 and results of calculations in coupled-channels approach. It is evident that at an ion energy of $^{16}O \leq 80$ MeV the subbarrier fusion cross sections, calculated using the Wong approximation or using the CCFUS software package disregarding the channel coupling, are going down much

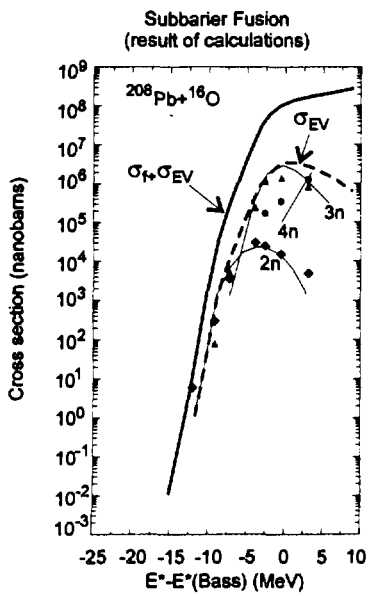

Fig.2.

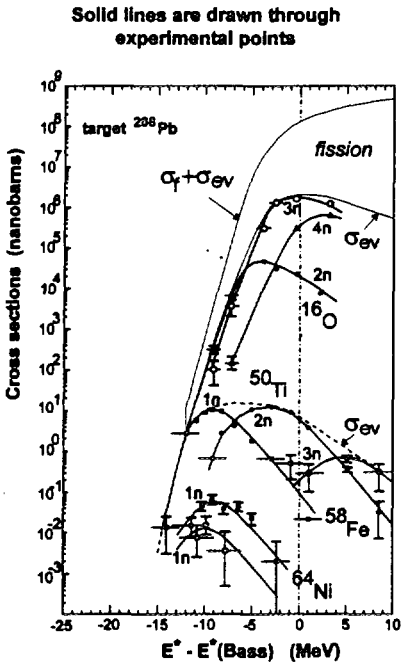

Fig.3

sharper and at an energy of $E^* = 72.5$ MeV are by nearly an order of magnitude lower than the experimental value of fusion cross section, whereas taking into account the channel coupling or zero-point vibrations leads to the increase of the cross section.

To analyse the fission and evaporation cross sections, we used a statistical model of the deexcitation process of compound nuclei which, for the sake of universality, uses the minimum number of physical assumptions and parameters [5]. It is shown that the evaporation reaction cross sections are well described in the framework of the statistical model taking into account shell effects according to Ignatyuk and it is also shown that such calculations, making use of only one set of model parameters, namely, the scaling factor to the liquid-drop barrier of Cohen, Plasil and Swiatecki $C = 0.65 + 0.7$ and the ratio of the level density parameters $\hat{a}_f/\hat{a}_\nu = 1.0$, correctly describe the cross sections of evaporation reactions in a wide range of compound nuclei up to superheavy elements. In this work the dependence of the nuclear mass shell correction on the energy in the level density parameter and the fission barrier were introduced in calculations [6], $C = 0.67$, $B_f(l=0) = 5.9$ MeV, respectively, and $l_{max} = 15$.

Figure 2 presents the comparison of the experimental data cross sections σ_{xn}, $\sigma_{ev} = \sigma_{xn} + \sigma_{pxn} + \sigma_{\alpha xn}$ and $\sigma_{ev} + \sigma_f$ with the results of calculations. The energy scale is presented as a difference between the excitation energy and Bass-barrier excitation energy $E^* - E^*$ (Bass). One can see from the figure that in spite of a wide range of cross sections

variations, the calculations reproduce well enough both the relative and absolute values of the cross sections. In the interval of excitation energies of 20-30 MeV, the contributions of the two fission chances to the total cross section are approximately equal, which has to be taken into account in the analysis of different characteristics of the fission process. It should be noted that our experimental values of evaporation cross sections differ by an order of magnitude from the data obtained in [3], but agree with the results of earlier work [7].

And finally, the study of deep subbarrier reactions using a Pb target is of special interest, since they form the basis for the synthesis of superheavy elements in cold fusion reactions [8]. Figure 3 presents the experimental fusion cross sections with ions of ^{16}O and much heavier ions of ^{50}Ti, ^{58}Fe, and ^{64}Ni (solid lines are drawn through experimental points) [8], and one can see that for the nuclei under consirderation there are no substantial changes of the fusion reaction threshold, despite the substantial growth of the Coulomb forces (from ^{16}O to ^{64}Ni). This is a good reason to think that additional extra-extra push energy has not been observed.

This work is supported in part by the Russian Fund of the Fundamental Investigation (Grants No.96-02-17743a and No.96-02-17209).

References

1. Oganessian Yu.Ts. et al. — JINR Rapid Communications, 1996, No.1[75]-96, p.123.
2. Andreyev A.N. et al. — Nucl. Instr. and Meth., 1995, v.A364, p.342.
3. Morton C.R. et al. — Phys. Rev., 1995, v.C52, p.243.
4. Itkis M.G. — In: Proc. of XV Nucl. Phys. Conf. LEND-95, St.Petersburg, April 18-22, 1995, ed. by Yu.Oganessian, W. von Oertzen, R.Kappakchieva, World Sci. Singapore, 1995, p.177.
5. Andreyev A.N. et al. — JINR Rapid Communications, 1995, No.4[72]-95, p.43.
6. Andreyev A.N. et al. — Yad. Fiz., 1990, v.52, p.640.
7. Vulgaris E. et al. — Phys. Rev., 1986, v.V33, p.2017.
8. Oganessian Yu.Ts., to be published in Proc. of the Int. Conf. on Nucl. Phys. «Structure of Vacuum and Elementary Matter», Wilderness/George, South Africa, March 10-16, 1996.

Received on Octover 30, 1996.

XJ9700072

УДК 519.615.7+621.384.634.5

NUMERICAL OPTIMIZATION OF ACTIVELY SCREENED SC MAGNETS COIL GEOMETRIES

A.V.Fedorov, I.A.Shelaev

This work is concerned with numerical optimization of actively screened SC magnets coil. An additional SC coil is suggested to shield stray fields. This SC coil only slightly increases the superconductor volume but drastically reduces the total magnet weight and its cost, and permits one to avoid such unpleasant features of the cold yoke as an additional energy losses due to steel magnetization in a pulse mode and nonlinearities with steel saturation at high fields. We consider analytically the field of a shielded magnet and show how the volume of superconductor should be increased to get a complete active shielding. The design of SC coil geometries is performed by solving the optimization problem. Some results of actively screened dipole coil optimization are presented.

The investigation has been performed at the Laboratory of Computing Techniques and Automation, JINR.

Численное моделирование обмотки активно экранированных СП-магнитов

А.В.Федоров, И.А.Шелаев

Проводится численное моделирование активно экранированных СП-магнитов. Для экранировки поля вне магнита используется дополнительная СП-обмотка. Данная обмотка позволяет существенно уменьшить вес магнита и его стоимость и избежать потерь энергии и нелинейностей в магнитном поле вследствие насыщения ферромагнетика при сильных полях. Аналитически исследуется возможность полной экранировки магнитного поля с помощью введения дополнительной обмотки. Реальная геометрия обмотки получена путем решения задачи условной оптимизации. Представлены результаты моделирования.

Работа выполнена в Лаборатории вычислительной техники и автоматизации ОИЯИ.

1. Introduction*

In modern SC magnets the field strength and its quality are determined by a SC coil and its shape. Nevertheless, a cold steel yoke constitutes 80% and more of the magnet weight which significantly increases the magnet cost and time of its cool-down and warm-

*This work was supported by the RFBR under Grant No.95-01-01467a

up [1]. The steel yoke increases the magnet field only by 20—25%, and its main role is to shield stray fields. This task can be successfully resolved by an additional SC coil that only slightly increases the superconductor volume, but drastically reduces the total magnet weight and its cost, and permits one to avoid such unpleasant features of the cold yoke as an additional energy losses due to steel magnetization in a pulse mode and nonlinearities with steel saturation at high fields.

We consider analytically the field of a shielded magnet and show how the volume of superconductor should be increased to get a complete active shielding. The design of SC coil geometries requires solving the sophisticated optimization problem [2]. We present some results of actively screened dipole coil optimization.

2. Ideal Screened Fields

Dipole and quadrupole fields required in high energy accelerators are produced by SC coils of two shapes [3]: overlapping ellipses and $\cos\theta$ for a dipole field and crossed ellipses or $\cos 2\theta$ for a quadrupole one which provide ideal fields. Let us consider an elliptical conductor with axes a, b and a current density j immersed into a bigger or screening one with axes a_s, b_s and a current density j_s. The magnetic field outside this pair of conductors is equal to [4]

$$B_{out} = \mu_0 \left(\frac{jab}{z + \sqrt{z^2 - c^2}} + \frac{j_s a_s b_s}{z + \sqrt{z^2 - c_s^2}} \right).$$

This equation shows that the outside field is zero if the following two conditions are fulfilled

$$jab = -j_s a_s b_s, \tag{2.1}$$

$$c = c_s. \tag{2.2}$$

Eq. (2.2) means that the total currents in both conductors are the same but of opposite directions, and from (2.3) it follows that the focuses of both elliptical conductors coincide. Now suppose that

$$a_s = ka \quad \text{and} \quad k > 1.$$

Then according to Eq. (2.2) and (2.3), we find

$$j_s = -j\frac{b}{k\sqrt{b^2+(k^2-1)a^2}} \approx -\frac{j}{k^2}. \tag{2.3}$$

The last approximation is valid if $a \approx b$ and $k >> 1$. This pair of screened conductors is used below to construct ideal screened fields.

If we now take another pair of similar conductors with as opposite currents as before and overlap (or cross) them, we shall get an ideal dipole (quadrupole) magnet without stray fields. Then the dipole field of the screened magnet is equal to

$$B_{ys} = -\frac{\mu_0 jbs}{a+b}\left[1-\frac{a+b}{k(ka+b_s)}\right] = B_y(1-h), \quad B_{xs}=0$$

The gradient G inside the screened quadrupole lens equals

$$G_s = -\mu_0 j\frac{a-b}{a+b}\left[1-\frac{b}{kb_s}\left(\frac{a+b}{a_s+b_s}\right)^2\right] = G(1-g).$$

Here dimensionless values of h and g show how much the field and gradient of screened magnets differ from the same value of unscreened coils. Evidently, a minimal value of k is $1+s/a$, where s is a distance between centres of the coil pairs. If we choose larger k, then there will be enough a current free space between screening conductors and a main coil to place there force collars that constrain coil motion to negligible levels. The area S of the main dipole coil is equal to

$$S = 2ab\left(\arcsin\frac{s}{2a}+\frac{s}{2a}\sqrt{1-\frac{s^2}{4a^2}}\right) \approx 2bs\left(1-\frac{s^2}{24a^2}\right).$$

The total current in this coil or its ampere-turns Iw are then $Iw = jS$. From this equation and equation (2.3) it follows that the same value for the screening coil Iw_s is

$$Iw_s \approx \frac{Iw}{k}. \tag{2.4}$$

The field strength at the screening coil is very low, and so the critical current density in it is 3—5 times higher than in the main coil. Therefore, the total additional volume of the superconductor in this coil needed for a complete screening is of the order of 10% of the superconductor in the main coil if k is equal to 2.5 and more.

A SC volume needed to screen a quadrupole lens is even lower. The cross section area S_m of its main coil equals

$$S_m = 2ab\left(\arccos\sqrt{\frac{1-e^2}{2-e^2}} - \frac{\pi}{4}\right) \approx \frac{c^2}{2}\sqrt{1-e^2},$$

where $e = ca^{-1}$ is the coil ellipticity. The area of the screening coil is

$$S_s \approx \frac{c^2}{2}\sqrt{1-\frac{e^2}{k^2}}$$

or almost the same as the main coil area. Therefore, Eq.(2.4) in the case of a quadrupole takes the form

$$Iw_s \approx -\frac{Iw}{k^2}.$$

It reflects the fact that a field outside a dipole drops with a distance r as r^{-2}; and outside a quadrupole, as r^{-3}. So the additional SC volume for screening a quadrupole is lower than in the case of a dipole.

3. Dipole with Shielding Coil

The determination of real screened dipole coil geometries is performed in two steps. First, we design the main coil to produce 5T magnetic field with low multipole content. Then kept constant the geometry of main coil we design the shielding coil to screen the field outside the magnet.

Let us consider in cylindrical coordinates r, θ, z, $0 \le \theta \le \frac{\pi}{2}$, M infinitely long straight conductors. Dipole symmetries are implied. Cross section of these conductors has angular positions $\varphi_m - \Delta_m$ and $\varphi_m + \Delta_m$, radial positions R_1^m and R_2^m, $m = 1, ..., M$. Let $r^+ \le \min(R_1^m)$, $r^- \ge \max(R_2^m)$, then for $r < r^+$ magnetic field $B^+(r, \theta)$ inside the aperture due to currents j_m in conductors is described by multipole expansion

$$B^+(r, \theta) = B_y^+ + iB_x^+ = -B_0\left[1 + \sum_{n=1}^{\infty} a_{2n}^+ e^{2n\theta i}\right]$$

$$B_0 = \frac{4\mu_0}{\pi}\sum_{m=1}^{M} j_m(R_2^m - R_1^m)\sin\Delta_m \cos\varphi_m$$

$$a_{2n}^{+} = \frac{4\mu_0}{\pi} \frac{r^{+}}{B_0} \frac{1}{4n^2 - 1} \left(\frac{r}{r^{+}} \right)^{2n} \sum_{m=1}^{M} j_m \left[\left(\frac{r^{+}}{R_1^m} \right)^{2n-1} - \left(\frac{r^{+}}{R_2^m} \right)^{2n-1} \right] \times$$

$$\times \sin (2n+1) \Delta_m \cos (2n+1) \varphi_m .$$

Magnetic field $B^{-}(r, \theta)$ outside the magnet is described for $r > r^{-}$ by

$$B^{-}(r, \theta) = B_y^{-} + iB_x^{-} = \sum_{n=1}^{\infty} a_{2n}^{-} e^{2n\theta i}$$

$$a_{2n}^{-} = \frac{4\mu_0}{\pi} r^{-} \frac{1}{4n^2 - 1} \left(\frac{r^{-}}{r} \right)^{2n} \sum_{m=1}^{M} j_m \left[\left(\frac{R_2^m}{r^{-}} \right)^{2n+1} - \left(\frac{R_1^m}{r^{-}} \right)^{2n+1} \right] \times$$

$$\times \sin (2n-1) \Delta_m \cos (2n-1) \varphi_m .$$

The main coil geometries design is considered as an optimization problem with objectives:

- main dipole field of 5T,
- minimization of multipole field — a_{2n}^{+}, $n = 1, ..., N^{+}$.

For dipole with shielding coil we add the objective of

- minimization of outside magnetic field — a_{2n}^{-}, $n = 1, ..., N^{-}$.

The design variables for this optimization problem are φ_m, Δ_m, j_m, $m = 1, ..., M$. Optimization was carried out by NAG Fortran Library routine E04UPF for $M = 6$, $N^{+} = N^{-} = 4$. Geometric parameters of the coil and obtained values of designed variables are presented in Table 1. Table 2 gives the multipole field content for this coil.

Magnetic flux lines and screening effects are depicted in Fig.1. Figure 2 represents total additional volume of superconductor needed for shielding coil (S_a) (in per cent of main coil superconductor volume) in dependence on current density ratio $\frac{j_s}{j_m}$ and on coils radius ratio $\frac{R_s}{R_m}$.

The results above show that SC dipole magnet with low stray fields can be constructed in two-dimensional case. The total additional volume of the superconductor is well described by the formulae

$$S_a = \frac{R_m}{R_s} \frac{j_m}{j_s} S_m ,$$

where S_m is the main coil superconductor volume.

Table 1. Actively screened dipole coil parameters

\m	1	2	3	4	5	6
Δ (rad)	0.514	0.098	0.252	0.063	0.366	0.124
φ (rad)	0.514	1.210	0.252	0.666	0.366	1.030
R_1 (mm)	25	25	35.5	35.5	100	100
R_2 (mm)	35	35	45.5	45.5	101	101
j (A/mm^2)	470	470	470	470	1053	1053

Table 2. Multipole field content for actively screened dipole

2n	$a^+_{2n} \times 10^{-4}$, $r = 15$ mm	$a^-_{2n} \times 10^{-4}$, $r = 120$ mm
2	1.0066	0.0083
4	0.0006	0.0000
6	– .0002	– .0032
8	0.0000	0.0024
10	0.3920	29.6644
12	– .3395	13.7798

To optimize coil ends, 3D magnetic field calculations were carried out. Obtained early coil geometries are used in calculations.

Magnetic field due to current **j** in coil Ω_c is described by Biot Savart law

$$\mathbf{B} = \frac{\mu_0}{4\pi} \int_{\Omega_c} \mathbf{j} \times \nabla \frac{1}{R} d\Omega.$$

To calculate **B** we approximate the domain Ω_c by tetrahedral elements with plane faces. Current density **j** is assumed to be a constant vector within the element. Then the evaluation of integral over the domain Ω_c is reduced to summation of integrals over elementary tetrahedrons. Last integrals are evaluated analytically. The magnet coil consist of straight

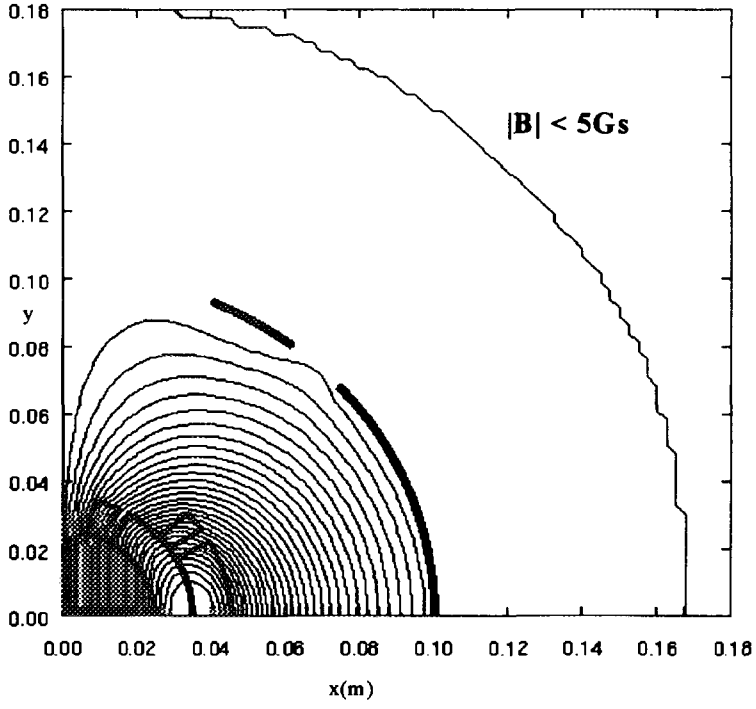

Fig.1. Magnetic field flux lines and screening effects for actively screened dipole

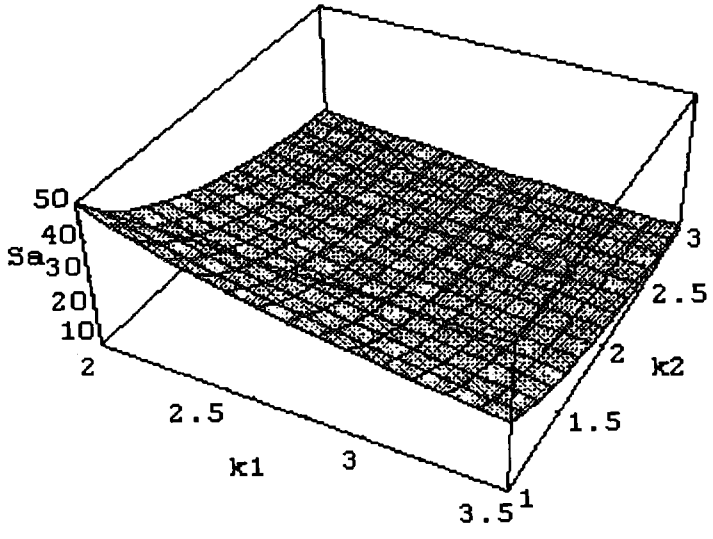

Fig.2. Additional volume of superconductor for actively screened dipole (in per cent of main coil superconductor volume). $k1 = S_s/S_m$, $k2 = j_s/j_m$

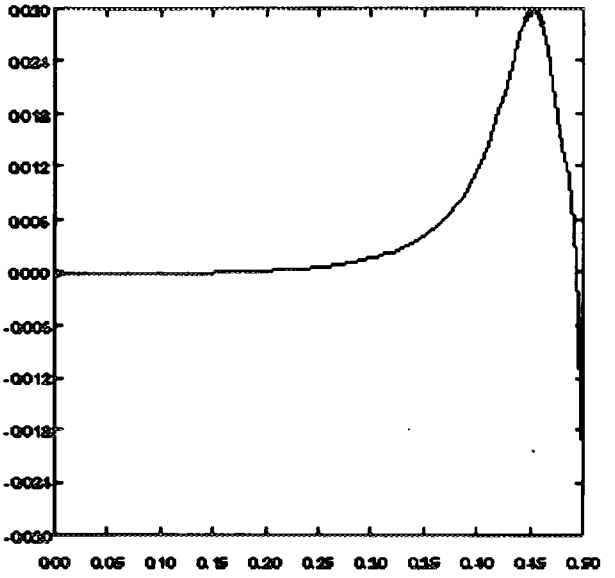

Fig.3. Magnetic field uniformity along the axis of actively screened dipole

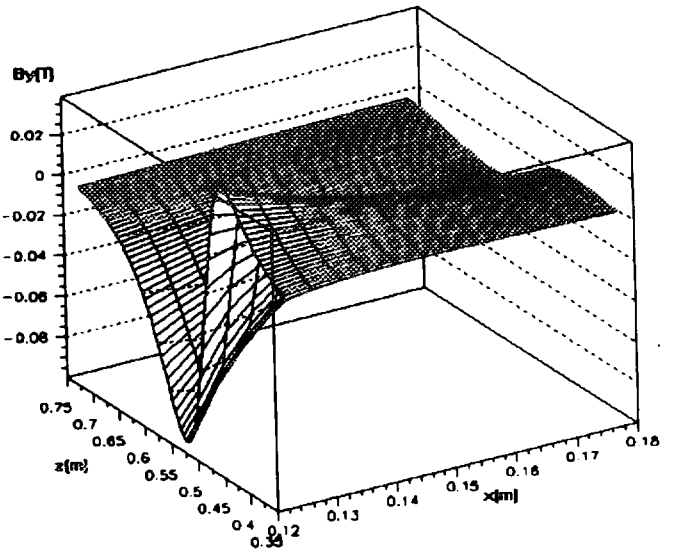

Fig.4. Stray fields in coil end region

Table 3. Actively screened dipole coil ends parameters

\m	1	2	3	4	5	6
d_m (cm)	100.	92.	100.	100.	96.	96.
α_m	1.	1.	1.	1.	0.4	0.4

Table 4. Peak field in actively screened dipole coil blocks

\m	1	2	3	4	5	6
$\|\mathbf{B}\|$ (T)	5.82	5.48	2.62	3.95	1.75	1.73

parts specified by its length d_m, $m = 1, ..., M$ and coil ends specified by its ellipticity α_m, $m = 1, ..., M$. Straight parts and ellipticity of shielding coil blocks are the design variables for coil ends optimization. Two partially contradictory objectives are imposed

- to remain the field uniformity on z axis inside the magnet,
- to screen field outside the magnet.

Field uniformity inside the magnet and magnetic field on median plane outside the magnet are depicted on Figs.3 and 4 for parameters d_m, α_m from Table 3. Table 4 gives the coil blocks peak field.

As it was expected a priori the screening on the magnet end is not so complete than in 2D case but field level is lower than one from the ends of main coil.

4. Conclusions

The results presented here show that wholly screened ironless SC dipoles and quadrupoles may be constructed and successfully used in high energy accelerators. SC magnets of this type are five times lighter per unit length and have two times and more smaller dimensions. It means that the cost of magnet operation could be decreased due to reduced cooling power.

Moreover, these magnets may be used in a collider when two magnets are placed in one cryostat side by side or «two-in-one». The fringing fields of one magnet lower than 5Gs will not disturb the field in the neighbour one. To reach this value it needs to place axes of both magnets at a distance of 4.5—5 radius of the aperture.

References

1. Fisk H.E. — Superconducting Magnets. Proc. of XIII Int. Conf. on High Energy Accelerators, Novosibirsk, Nauka, 1987, v.2, p.15.
2. Russenschuck S. — A Computer Program for the Design of Superconducting Accelerator Magnets. CERN AT/95-39 (MA), Geneva, 1995.
3. Wilson M.N. — Superconducting Magnets. Calderon Press, Oxford, 1983, p.29.
4. Shelaev I.A. — JINR Rapid Communications, 1994, No.4[67]-94, p.50.

Received on October 8, 1996.

XJ9700073

УДК 539.17

NARROW RESONANCES IN THE SYSTEM OF TWO π^--MESONS

Yu.A.Troyan, V.N.Pechenov, E.B.Plekhanov*, A.Yu.Troyan
LHE, Joint Institute for Nuclear Research, Dubna
S.G.Arakelian
Lebedev Physics Institute (Russian Academy of Sciences), Moscow
V.I.Moroz, A.P.Ierusalimov
LCTA, Joint Institute for Nuclear Research, Dubna

The study of the production of exotic 4-quark resonances with isotopic spin $I = 2$ in the $\pi^-\pi^-$-systems from the reaction $np \to pp\pi^+\pi^-\pi^-$ was carries out using the data obtained in the irradiation of 1m H_2 bubble chambers of LHE, JINR by neutrons at the momentum $P_n = 5.20 \pm 0.13$ GeV/c. A number of enhancements were found at the masses of 0.330; 0.354; 0.397; 0.447; 0.510; 0.569; 0.650; 0.736; 0.822, and 0.920 GeV/c^2. Experimental widths of resonances are comparable with the resolution that is linearly increasing from 1.4 to 15.0 MeV/c^2 (σ_{res}) under alteration of masses from the sum of masses of pions to ≈1 GeV/c^2. An attempt was made to determine the spins of resonances. For the resonances at the mass of 0.397 GeV/c^2, the most probable value of spin was proved to be equal to $J \geq 6$.

The investigation has been performed at the Laboratory of High Energies, JINR.

УЗКИЕ РЕЗОНАНСЫ В СИСТЕМЕ ДВУХ π^--МЕЗОНОВ

Ю.А.Троян и др.

В реакции $np \to pp\pi^+\pi^-\pi^-$, выделенной на материалах облучения 1 м жидководородной пузырьковой камеры ЛВЭ ОИЯИ нейтронами с импульсом $P_n = 5{,}20 \pm 0{,}13$ ГэВ/с, исследовано образование экзотических четырехкварковых резонансов с изотопическим спином $I = 2$ в системе двух π^--мезонов. Обнаружен ряд особенностей с массами 0,330; 0,354; 0,397; 0,447; 0,510; 0,569; 0,650; 0,736; 0,822 и 0,920 ГэВ/c^2. Экспериментальные ширины резонансов определяются экспериментальным разрешением по массам, которое линейно растет от 1,4 до 15,0 МэВ/c^2 (σ_{res}) при измерении масс от суммы масс двух π^--мезонов до ≈1 ГэВ/c^2. Сделана попытка определения спинов резонансов. Для резонанса с массой 0,397 ГэВ/c^2 наиболее вероятное значение спина оказалось равным $J \geq 6$.

Работа выполнена в Лаборатории высоких энергий ОИЯИ.

* E-mail address: plekhano@cv.jinr.ru

The first results of the study of resonances in $\pi^-\pi^-$-system from the reaction $np \to pp\pi^+\pi^-\pi^-\pi^0$ (5712 events) at $P_n = 5.20 \pm 0.13$ GeV/c were reported at the X International Seminar on Problems of High Energy Physics [1]. The data were obtained in an exposure of 1 m H_2 bubble chamber of LHE JINR by monochromatic neutrons. The beam parameters, the methods of identification of reaction channels, the values of cross sections, etc., were published in paper [2].

In this report, we present the results of the study of two π^--mesons system from the reaction (1) at the same neutron momentum (total, 8394 events of reaction (1) were identified).

$$np \to pp\pi^+\pi^-\pi^-. \qquad (1)$$

The distribution of the effective masses of $\pi^-\pi^-$-combinations from the reactions (1) is shown in Fig.1. The distribution is approximated by an incoherent sum of the background curve taken in the form of a superposition of Legendre polynomials of up to fourth power inclusive (coefficient of higher power polynomials are negligible), and by ten Breit — Wigner resonance curves. The part of the background is equal to 91%. The background

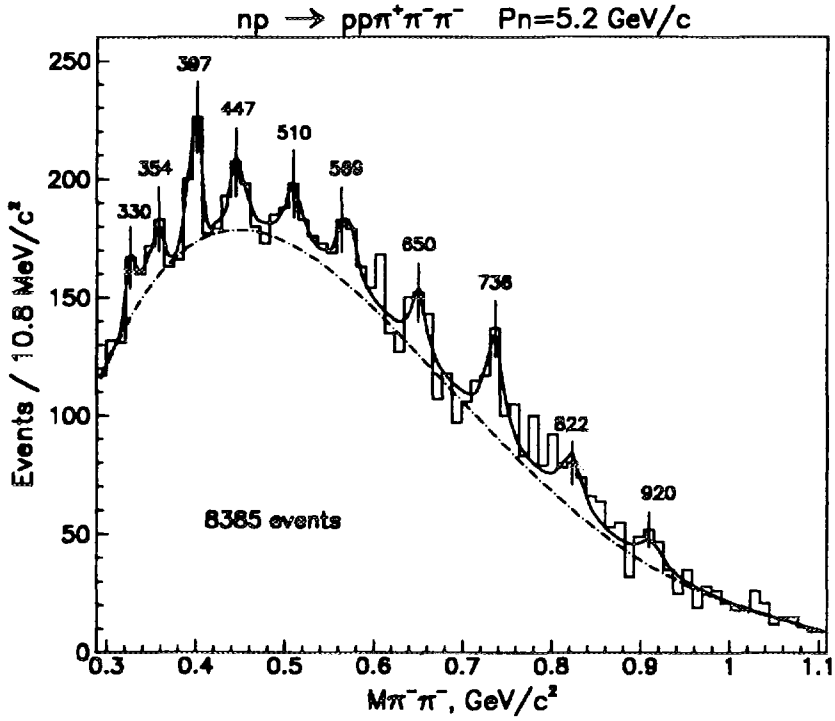

Fig.1. The effective mass distribution of $\pi^-\pi^-$-combinations at P_n = 5.2 GeV/c

describes the region outside the resonances with $\chi^2 = 1.01 \pm 0.14$; $\sqrt{D} = 1.37 \pm 0.10$, that is very close to the pure statistical distribution ($\chi^2 = 1$; $\sqrt{D} = 1.41$).

The obtained data are presented in the Table.

Table

$M_e \pm \Delta M_e$ MeV/c^2	$\Gamma_e \pm \Delta\Gamma_e$ MeV/c^2	$\Gamma_R \pm \Delta\Gamma_R$ MeV/c^2	$\sigma \pm \Delta\sigma$ μb	S.D.	P
330 ± 6	$12.1^{-2.8}_{+5.8}$	$11.1^{-2.8}_{+5.8}$	2.5 ± 1.2	2.2	$8.4 \cdot 10^{-1}$
354 ± 6	$12.1^{-2.7}_{+5.3}$	$10.5^{-2.7}_{+5.3}$	2.7 ± 1.3	2.3	$7.6 \cdot 10^{-1}$
397 ± 6	$12.1^{-1.7}_{+2.5}$	$9.3^{-1.7}_{+2.5}$	5.4 ± 1.4	4.4	$1.6 \cdot 10^{-4}$
447 ± 7	$17.6^{-9.4}_{+31.3}$	$14.6^{-9.4}_{+31.3}$	4.2 ± 1.7	2.7	$9.0 \cdot 10^{-2}$
510 ± 7	$21.6^{-8.8}_{+25.7}$	$17.6^{-8.8}_{+25.7}$	4.2 ± 1.9	2.4	$1.9 \cdot 10^{-1}$
569 ± 7	$22.0^{-10.2}_{+27.9}$	$16.1^{-10.2}_{+27.9}$	4.2 ± 1.6	2.9	$4.6 \cdot 10^{-2}$
650 ± 8	$19.3^{-10.4}_{+45.3}$	$5.9^{-5.9}_{+45.3}$	4.5 ± 1.4	3.4	$7.1 \cdot 10^{-3}$
736 ± 6	$22.8^{-7.4}_{+13.7}$	$6.0^{-6.0}_{+13.7}$	7.8 ± 1.7	5.4	$1.8 \cdot 10^{-9}$
822 ± 9	$27.2^{-8.6}_{+15.7}$	$9.2^{-8.6}_{+15.7}$	5.8 ± 1.4	3.7	$2.2 \cdot 10^{-3}$
920 ± 7	$30.5^{-18.0}_{+108.7}$	$6.9^{-6.9}_{+108.7}$	2.4 ± 0.8	3.5	$5.4 \cdot 10^{-3}$

The first column contains the central value of the resonance mass; the second one, the experimental full width of the resonance; the third one, the true resonance width, obtained by quadratic subtraction of the width of the resolution function for the masses of $\pi^-\pi^-$-combinations from the experimental widths. In the fourth colum, the cross section of the resonance production in reaction (1) is given (see [2]); in the fifth column, number of standard deviations above the background; in the sixth column, probability (multiplied by the number of bins) that observed enhancements is due to background fluctuations.

The experimental resolution for the masses $\sigma_{res}(M)$ is well approximated by formula (2):

$$\sigma_{res} = 2.1 \cdot [(M - M_0)/0.1] + 1.4, \qquad (2)$$

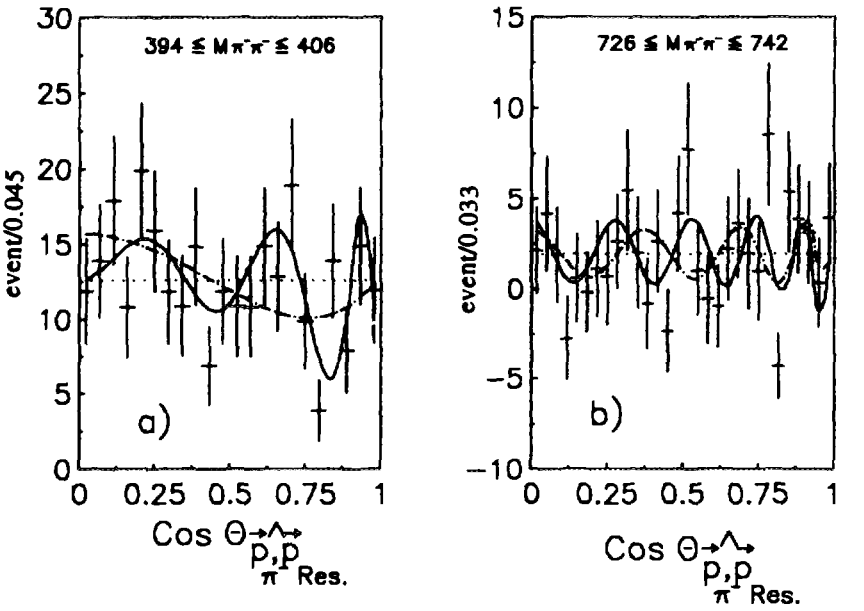

Fig.2. a) The distribution of cos $\Theta_{\widehat{P_{\pi^-}, P_{Res}}}$ for resonance at the mass of 397 MeV/c^2 and b) for resonance at the mass of 736 MeV/c^2

where M is effective mass of a resonance (in GeV/c^2); M_0, the mass of two π^--mesons (in GeV/c^2). The result for σ_{res} is given in MeV/c^2. On can see from formula (2) that the mass resolution is linearly increasing from 1.4 to 15.0 MeV/c^2 under alteration of masses from the sum of masses of two pions to ≈1 GeV/c^2.

To determine the spins of resonances there is analysed the distribution of cos $\Theta_{\widehat{P_{\pi^-}, P_{Res}}}$ — the angle between the direction of motion of π^--meson from the resonance decay ($\mathbf{P}_{\pi^-}$) and the direction of resonance motion ($\mathbf{P}_{Res}$) in general c.m.s.. All quantities are taken in resonance c.m.s. (helicity coordinate system). It is known for strong decays that such distributions can be described by a sum of Legendre polynomials of an even power with the maximum powers of $2J$, where J is the resonance spin [3].

The distributions of cos $\Theta_{\widehat{P_{\pi^-}, P_{Res}}}$ are shown in Fig.2a for the resonance at the mass of 397 MeV/c^2: dotted line is isotropic distribution; dash-dot line is the description by Legende polynomials of up to the fourth power inclusive; solid line, description by Legendre polynomials of up to 12 power inclusive. The corresponding confidence levels are equal to 2.5%; 8.3%, and 45.3%, respectively. Hence, one can conclude the spin of the resonance in $\pi^-\pi^-$-system at the mass of 397 MeV/c^2 $J \geq 6$. In this procedure, the

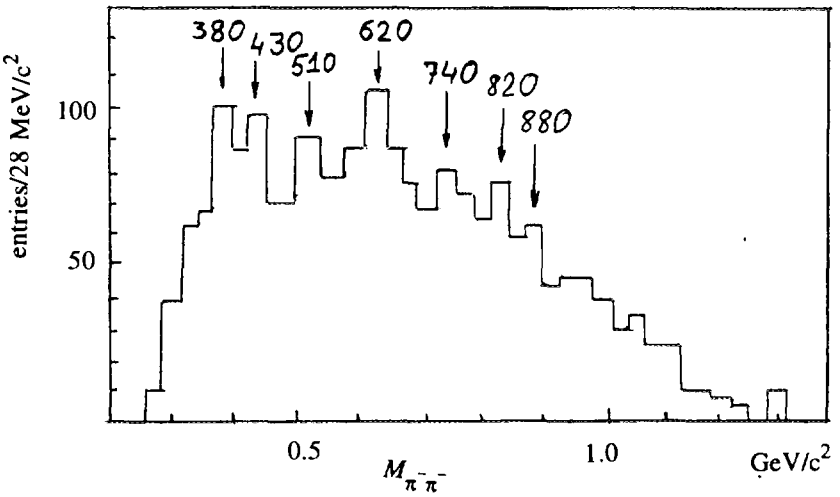

Fig.3. The effective mass distribution of $\pi^-\pi^-$-combinations from the reaction $\bar{p}d \to 2\pi^-2\pi^+n$ [6]

background from the left and from the right is not subtracted, because it is essentially isotropic.

The distributions of cos $\Theta_{\widehat{P_{\pi^-}P_{Res}}}$ are shown in Fig.2b for the resonance at the mass of 736 MeV/c^2: dotted line is the isotopic distribution; dash-dot line, description by Legendre polynomials of up 16 power inclusive; solid line, description by Legendre polynomials of up to 22 power inclusive. The corresponding confidence levels are equal to 19.4%; 32.5%, and 55.8%, respectively. Hence, one can conclude the spin of the resonance in $\pi^-\pi^-$-system at the mass of 736 MeV/c^2 $J > 1$. In this procedure, the background from the left and from the right is subtracted.

We refer to survey article [4] devoted to theoretical discussion of the problem of 4-quark resonances and present experimental situation. There are few experimental data in literature concerned with a study of similar resonances in this region of effective masses (from $2m_\pi$ to $\approx$1 GeV/c^2) [5,6].

It needs to note the results obtained by OBELIX collaboration [6]. Figure 3 shows the effective mass distribution of $\pi^-\pi^-$-combinations from the reaction $\bar{p}d \to 2\pi^-2\pi^+n$. The arrows mark the following peculiarities in the effective masses spectrum: 0.38; 0.43; 0.51; 0.62; 0.74; 0.82; 0.88 GeV/c^2. One can see a good coincidence (taking into account errors) between these peculiarities and our narrow resonance structures in the effective masses spectrum of $\pi^-\pi^-$-combinations from the reaction (1). The author of the paper [6] did not pay attention to these peculiarities in the distribution presented in Fig.3. It is necessary to

note this distribution is plotted using a little statistics and by larger bins (28 MeV/c^2) than in Fig.1.

We are grateful to Dr. V.L.Lyuboshitz for help in this work and Dr. M.G.Sapozhnikov for valuable remarks.

References

1. Troyan Yu.A. et al. — Proc. of Seminar on High Energy Phys. Probl. Relat. Nucl. Phys. and Quantum Chromodynamics, Dubna, September, 1990, p.149; IPNO-DRE 91-18.
2. Besliu C. et al. — Yad. Fiz., 1986, vol.43, p.888.
3. Baldin A.M. et al. — Kinematics of Nuclear Reactions. Atomizdat, M., 1968.
4. Achasov N.N., Shestakov G.N. — UFN, 1991, vol.161, p.53.
5. Albrecht H. et al. — Phys. Lett., 1991, vol.B260, pp.259—264.
6. Ableev V.G. et al. — Nucl. Phys., 1995, vol.A585, pp.577—617.

Received on November 1, 1996.

XJ9700074

УДК 539.1.074.8 + 539.1.074.9

NEW METHOD OF ANALYSIS OF INTERMEDIATE ENERGY NEUTRON SPECTRA (1 keV ≤ E_n ≤ 100 keV)

Yu.P.Popov, P.V.Sedyshev, M.V.Sedysheva

The new method of intermediate energy neutron spectrometry is proposed. The method is based on the analysis of the γ-line shape of the primary transition during capture of the investigated neutrons in a special converter. This method allows both pulsed and continuous neutron fluxes (fields) to be analysed.

The investigation has been performed at the Laboratory of Neutron Physics, JINR.

Новый метод анализа спектров нейтронов промежуточных энергий (1 кэВ ≤ E_n ≤ 100 кэВ)

Ю.П.Попов, П.В.Седышев, М.В.Седышева

Предлагается новый метод спектрометрии нейтронов промежуточных энергий, основанный на анализе формы γ-линии первичного перехода при захвате исследуемых нейтронов специальным конвертером. Метод позволит анализировать как импульсные, так и стационарные нейтронные потоки (поля).

Работа выполнена в Лаборатории нейтронной физики ОИЯИ.

The new method for analysis of spectra of intermediate energy neutrons, i.e., over the 1—100 keV energy interval, is described. The method is based on the idea of how to study the resolution of time slowing-down spectrometers over the keV energy interval suggested by one of the authors of [1]. In principle, intermediate energy neutron spectra can be investigated by the time-of-flight method, but this is only possible at pulsed neutron sources with a nanosecond range. Other methods of spectra analysis of neutron flux (field) shapes applied for investigations of fast neutrons, including the proton recoil method, measurement of the energy of emitted charged particles following a capture of the investigated neutrons, threshold reactions, etc., (see [2]) do not practically work in the intermediate energy region.

The reported method is based on the determination of the γ-line shape of the germanium γ-spectrometer used to register **primary** gamma-ray transitions during radiative capture of intermediate energy neutrons in a special converter. When energy dispersion of the captured neutrons is approximately equal to or larger than the energy resolution of the γ-spectrometer, the shape of the γ-line amplitude is distorted due to difference in the captured neutron energies, i.e., a change in the excitation energy of decayed nucleus states in the converter material at a fixed final state of the measured γ-transition.

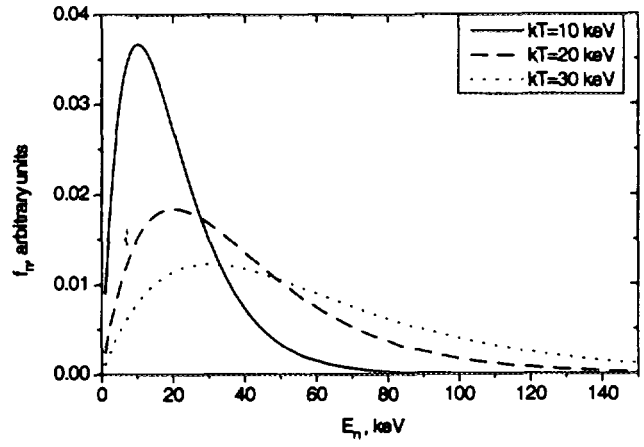

Fig.1. Maxwellian neutron spectra

If an intense (and hence, $E1$-multipolarity) primary γ-transition with the energy $E^i_{\gamma 0}$ to the i-th final level of the excited nucleus appears following a thermal neutron capture ($E_n \cong 0$) by a converter nucleus with the atomic weight A, the energy of an analogous transition following the capture of an E_n neutron is:

$$E^i_\gamma = E^i_{\gamma 0} + [A/(A+1)] \cdot E_n. \quad (1)$$

As a converter, one is recommended to use an isotope with a smooth behaviour of the partial (for the given γ-transition) capture cross section of neutrons from the investigated spectrum. This can be the cross section of a partial transition following a direct radiative capture (light or nearly magic nuclei) or the radiative neutron capture cross section averaged over many neutron resonances. In the latter case, it is necessary to have the converter with an average level spacing $D \ll 1$ keV. Then the energy dependence of the averaged partial capture cross section of neutrons with an orbital momentum $l = 0$ (s-neutrons) is (see, e.g., [3]):

$$\langle \sigma^i_{n\gamma}(E_n) \rangle_s \sim E_n^{-1/2}. \quad (2)$$

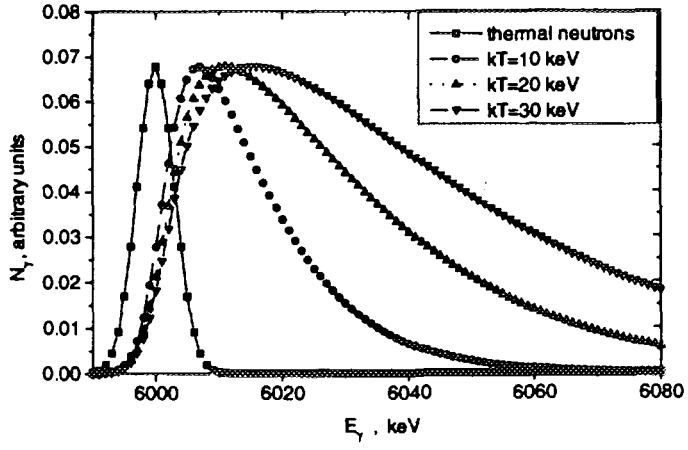

Fig.2. The 6 MeV γ-line shapes registered by the Ge(Li)-detector for the capture of the neutrons from Maxwellian spectra, as well as thermal neutrons

Since the gamma-registration efficiency and the resolution power of the spectrometer for captured neutrons are practically constant ($E^i_{\gamma 0}$ is about 5 MeV and its variations do

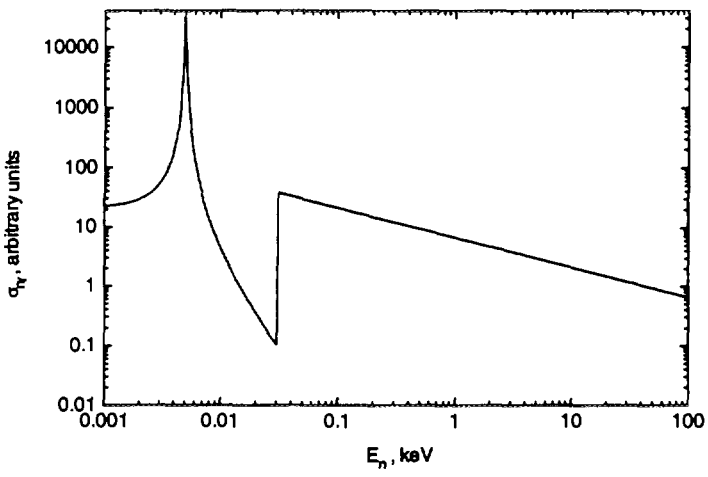

Fig.3. The energy dependence of the capture cross section of a converter

not exceed 100 keV), the amplitude spectrum of the γ-line is a product of the neutron flux $f_n(E_n)$ by the partial capture cross section, both being the functions of neutron energy. The observed spreading of the product is governed by the spectrometer resolution function $\varphi_0(E_\gamma)$ for γ-lines from thermal neutron capture

$$N_\gamma(E_\gamma)dE_\gamma = k \cdot \varphi_0(E_\gamma)dE_\gamma \cdot \langle\sigma(E_n)\rangle \cdot f_n(E_n), \qquad (3)$$

where the coefficient k is determed by the experimental geometry, registration efficiency and the measurement time, and E_γ differs from E_n by a constant (see (1)).

The computer modelled results obtained with the proposed method are presented in Figs. 1 and 2. The Maxwellian neutron spectra at temperatures kT = 10, 20, 30 keV are shown in Fig.1. Figure 2 represents the correspondig responses of the Ge(Li) spectrometer with the resolution 4 keV for the 6 MeV γ-transition energy. The calculations were performed for the converter made of the material with neutron resonance parameters like those of gold. The energy dependence for the radiative capture cross section is shown in Fig.3. In calculations, we only used the energy dependence of *s*-wave neutrons.

To obtain the shape of the neutron flux energy distribution, it is necessary to solve an inverse problem for equation (3).

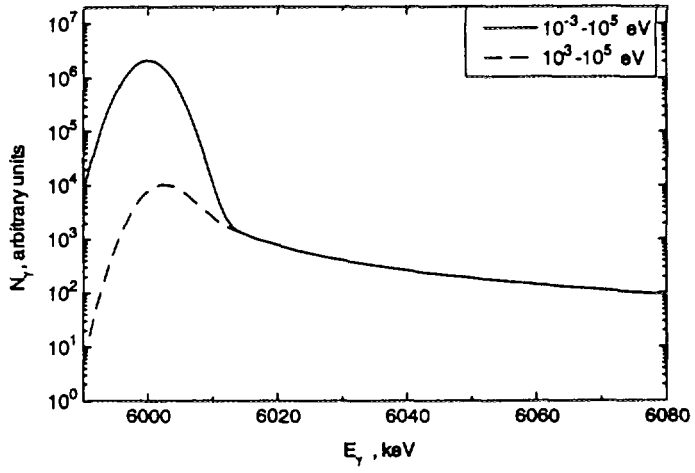

Fig.4. The same as in Fig.2, for the neutron spectrum with the $1/E_n$ distribution over two energy regions

According to preliminary estimation of the efficiency of this method to register one γ-quantum, about $10^3 - 10^4$ neutrons captured in the converter are needed. At the same time, the registered γ-quantum does not only indicate that a capture event has occurred but also provides information on the energy of the captured neutron. The proposed method, unlike the time-of-flight method, does not need long flight paths which reduce the efficiency of the method by several orders of magnitude (e.g., the flight path of 30 m allows one to use only 10^{-7} of the total neutron flux).

The proposed method can be used to analyse fluxes from stationary or pulsed neutron sources both inside and outside different moderators and other construction materials. Figure 4 illustrates the γ-shape at 6 MeV observed following capture of neutrons with the energy distribution $f_n(E_n) \sim 1/E_n$.

The method can by very useful for dosimetry of intermediate energy neutrons, for protection physics, as well as for investigations of averaged cross sections for partial γ-transitions.

References

1. Popov Yu.P. — JINR Communication P3-80-672, Dubna, 1980 (in Russian); Popov Yu.P. — Sov. Jorn. Phys. Part. Nucl., 1995, v.26, p.628—636.
2. Abramov A.I., Kazansky Yu.A., Matusevich E.S. — Osnovy eksperimentalnykh metodov jadernoj fiziki, M.: Atomizdat, 1970, p.395 (in Russian).
3. Popov Yu.P., Fenin Yu.I. — ZhETF, 1962, v.43, p.2000.

Received on December 1, 1996.

Краткие сообщения ОИЯИ №6[80]-96

Учредитель и издатель — Объединенный институт ядерных исследований

Журнал зарегистрирован в Комитете по печати РФ

Регистрационное свидетельство № 013176 от 27.12.94

Редакторы: М.И.Зарубина, Э.В.Ивашкевич

Рукопись сборника поступила 19.12.96. Подписано в печать 16.01.96
Формат 70×100/16. Офсетная печать. Уч.-изд.листов 7,52
Тираж 620. Заказ 49644. Цена 9000 р.

141980 г. Дубна Московской области, ул.Жолио-Кюри, 6
Издательский отдел Объединенного института ядерных исследований